THESIS FOR THE DEGREE OF DOCTOR OF PHILOSOPHY

– i –

NANOFLUIDICS AS A TOOL FOR PARALLELIZED SINGLE NANOPARTICLE CHARACTERIZATION

FLUORESCENCE SINGLE NANOPARTICLE CATALYSIS AND SIZE DETERMINATION THROUGH 1D BROWNIAN MOTION

SUNE LEVIN

Department of Biology and Biological Engineering

CHALMERS UNIVERSITY OF TECHNOLOGY

Gothenburg, Sweden 2021

NANOFLUIDICS AS A TOOL FOR PARALLELIZED SINGLE NANOPARTICLE
CHARACTERIZATION - FLUORESCENCE SINGLE NANOPARTICLE CATALYSIS
AND SIZE DETERMINATION THROUGH 1D BROWNIAN MOTION
SUNE LEVIN
ISBN 978-91-7905-469-4

Department of Biology and Biological Engineering
Chalmers University of Technology
SE-412 96 Gothenburg
Sweden
Telephone + 46 (0)31-772 1000

Cover:
Illustration of single nanoparticle catalysis and fluorescent vesicles in nanochannels observed
with fluorescence microscopy. The different channels showcase the multitude of experiments
that are possible in this kind of nanofluidic experimental system.

NANOFLUIDICS AS A TOOL FOR PARALLELIZED SINGLE NANOPARTICLE CHARACTERIZATION

FLUORESCENCE SINGLE NANOPARTICLE CATALYSIS AND SIZE DETERMINATION THROUGH 1D BROWNIAN MOTION

SUNE LEVIN

Department of Biology and Biological Engineering
Chalmers University of Technology

Abstract

Nanoparticles exist widely in nature and are objects of study in many scientific disciplines due to their high performance in a wide range of applications. With modern techniques that facilitate creating and shaping of nanoparticles into ever more complex shapes and compositions, characterization of particle properties is essential. Nanoparticles are typically heterogeneous and techniques with single particle resolution are necessary to avoid the ensemble averaging that is otherwise prevalent. Plenty of methods have been developed to characterize single particle properties, but they all have their own restrictions and limitations, and additional methods are still needed to complement existing methods.

This thesis is based on two novel methods for single nanoparticle characterization. The first method, parallelized nanofluidic fluorescence microscopy, evaluates the fluorescence downstream of single Au nanoparticles, each one in its own nanochannel, to measure the turnover frequency during catalytic reduction at the particle surfaces. It facilitates measurements of catalytic turnover frequency from single Au nanoparticles of different sizes and shapes measured in a parallelized fashion to ensure identical reaction conditions and synchronous measurement. The second method, Nano-SMF, monitors the Brownian motion of fluorescent particles flowing through an array of nanochannels and determines the particle sizes based on the particle movement. It provides characterization of size and multiple fluorescence intensities for thousands of individual fluorescent particles with high throughput and for complex size distributions, which are prevalent in biological systems.

Both methods utilize nanofluidic flow systems to keep the readout signal in focus of the microscope and separate the nanoparticles and the signals emanated by them within parallel nanochannels. Together they showcase how nanofluidics provides a practical and versatile platform for single nanoparticle characterization.

Keywords: single nanoparticle catalysis, heterogenous catalysis, nanofluidics, particle tracking, Brownian motion, fluorescence microscopy, dark field microscopy

List of Publications

This thesis is based on the work contained in the following research papers:

I. **A nanofluidic device for parallel singe nanoparticle catalysis in solution**
<u>Sune Levin</u>, Joachim Fritzsche, Sara Nilsson, August Runemark, Bhausaheb Dhokale, Henrik Ström, Henrik Sundén, Christoph Langhammer, Fredrik Westerlund
Nature Communications, **10**, (2019), 4426.

II. **Size determination and multiplexed fluorescence-based phenotyping of single cell-derived membrane vesicles using a nanochannel device**
Quentin Lubart[1], <u>Sune Levin</u>[1], Stephan Block, Silver Jõemetsa, Erik Olsén, Sriram KK, André Görgens, Samir El-Andaloussi, Fredrik Höök, Marta Bally, Fredrik Westerlund, Elin K. Esbjörner
(Manuscript).

III. **Nanofluidic trapping of colloidal nanocrystals for parallelized single particle catalysis**
<u>Sune Levin</u>, Sarah Lerch, Astrid Boje, Joachim Fritzsche, Sriram KK, Henrik Ström, Anders Hellman, Kasper Moth-Poulsen, Henrik Sundén, Fredrik Westerlund, Christoph Langhammer
(Manuscript).

---

[1] Authors contributed equally to the work.

Contribution Report

Below follows a description of my contributions to the papers appended in this thesis.

I. Developed the nanofluidic device together with J.F., C.L. and F.W. Designed, performed, and evaluated experiments including catalysis measurements and simulations in 1D and analyzed the data. Wrote the paper with H.Su., C.L. and F.W.

II. Performed single particle tracking experiments and analysis for polystyrene beads, Au nanoparticles, and P-dots. Wrote MATLAB code to evaluate colocalization. Wrote the paper with Q.L., F.W. and E.K.E.

III. Designed the nanofluidic layout with J.F., F.W. and C.L. Designed, performed, and evaluated experiments including catalysis measurements and analyzed the data. Wrote the paper with H.Su., F.W. and C.L.

Preface

This dissertation was submitted for the partial fulfilment of the degree of Doctor of Philosophy. The original work presented in this dissertation was carried out between August 2016 and June 2021 at the Department of Biology and Biological Engineering, Chalmers University of Technology, under the supervision of Professor Fredrik Westerlund and with co-supervision from Professor Henrik Sundén and Professor Christoph Langhammer. The research was funded by Knut and Alice Wallenbergs Stiftelse and the European Research Council.

Sune Levin
June 2021

Table of Contents

1 Introduction

Nanoparticles are incredibly useful for a wide range of applications[1, 2]. Industrially, nanoparticles made of metals or metal oxides are prominent for use in, for example, solar energy[3], cancer treatment[4, 5], and catalysis[2, 6]. Nanoparticles can also be shaped from other materials, such as carbon[7], lipids[8], or polymers[9], and biological nanoparticles, such as exosomes, also occur naturally within our bodies and control cell function and communication[10, 11]. Their usefulness derives from an abundance of new material properties that arise, due to for example increased surface area, when the particle size is reduced to the nanometer scale[12]. There is therefore a need for nanoparticle characterization to understand and apply these new material properties efficiently. However, characterizing nanoparticles is complicated because of their small size and innate heterogeneity[13-18]. Traditionally they have been evaluated in ensembles of thousands to billions of particles to achieve high enough signals. However, measuring a multitude of particles as one and the same signal results in a particle average, where the individualities of the particles are lost. Due to the extensive heterogeneity generally seen among nanoparticles, characterization at the single particle level is needed to completely capture the particle properties and understand where the properties originate from.

In the last decades, a multitude of techniques, such as transmission electron microscopy[19] and electron beam lithography[20, 21] have made it possible to visualize and shape materials on the nanometer scale. These techniques have boosted the applicability and understanding of nanoparticles and built a platform for the field of nanotechnology. In addition, a multitude of techniques for measuring single nanoparticles properties have emerged[22-27], which expand our insight even further by avoiding ensemble averaging. While the understanding of nanoparticle properties has increased tremendously, there are still a lot of unanswered questions, and due to their heterogeneity, detailed single particle characterization is essential.

In this thesis, I present two methods for extracting single particle properties related to size, fluorescence intensity, and catalytic activity from single nanoparticles in a parallelized fashion. The first method I will refer to as parallelized nanofluidic fluorescence microscopy (**Paper 1 and 3**). It utilizes fluorescence microscopy and an array of parallel nanochannels to determine the catalytic turnover frequency for fluorescein reduction of tens of differently shaped single Au nanoparticles. The second method, Nano-SMF (SMF; size and multiplexed fluorescence), is used to determine the size and multiple fluorescence intensities for various particles with diameters down to 20 nm (**Paper 2**). Nano-SMF can be applied in many fields, but is here demonstrated for a biological application, i.e., the characterization of subpopulations within samples of fluorescent lipid vesicles and exosomes.

The aim of this thesis is to give a background into the fundamental science used in these two methods for nanoparticle characterization and present them in the context of state of the art techniques. Both methods utilize parallel nanochannels to achieve high throughput and keep the nanoparticles or fluorescent reactants in the microscope focus. I will therefore, in **Chapter 2**, give and overview of the field of nanofluidics and fabrication techniques used to create the nanochannel arrays. **Chapter 2** also covers fabrication and characterization of nanoparticles since nanoparticle properties are a core focus of both methods. Microscopy is used extensively in these methods, so the fundamentals of both fluorescence and dark field microscopy is comprised in **Chapter 3**. Since measuring single nanoparticle catalysis is the purpose of parallelized nanofluidic fluorescence microscopy, catalysis, and in particular heterogeneous catalysis, is described in **Chapter 4**. Nano-SMF utilizes the relation between Brownian motion and particle size to determine particle sizes from particle movement in the nanochannels. This is elaborated on in **Chapter 5**, where Nano-SMF is also presented in the context of other size determination techniques. Before discussing the way forward and future prospects for the two methods, in **Chapter 7**, I summarize the appended papers and elaborate on additional contributions in **Chapter 6**.

2 Nanostructures – fluidic devices and nanoparticles

In 1959 Richard Feynman famously stated, "There's plenty of room at the bottom" in his talk with the same name[28], when he envisioned the possibilities to shape materials down to the scale of atoms. Already then, it was possible to observe objects down to single nanometers through electron microscopy, but extensive manipulations at that scale were still decades away. Today, we all walk around with computers detailed down to a few nanometers in our pockets, and yet there seems to be room left for more. Shaping materials on the nanoscale has provided technological wonders and a deeper understanding to develop materials with more and more detail. It has also provided the foundation to create the nanofluidic devices and the nanoparticles crucial for the science in this thesis. In this Chapter, I will give an overview of nanofluidics and the various nanoparticles I have handled in my thesis, from fabrication to application and characterization.

2.1 Nanofluidics

Nanofluidics is the study and control of liquid and/or gas confined by structures where at least one dimension is in the nanometer scale (generally 1-100 nm)[29, 30]. However, the field of nanofluidics often extends into length scales of 100-1000 nm to allow for research on larger nanometric objects, such as single cells, nanoparticles, exosomes and DNA, in what is sometimes referred to as extended nanofluidics[31, 32]. Since nanofluidics is a field based on its very general concepts, such as fluids and small size, it is inherently interdisciplinary with broad use in all natural sciences[33]. The multitude of disciplines covered by nanofluidics is highlighted in Figure 2.1.

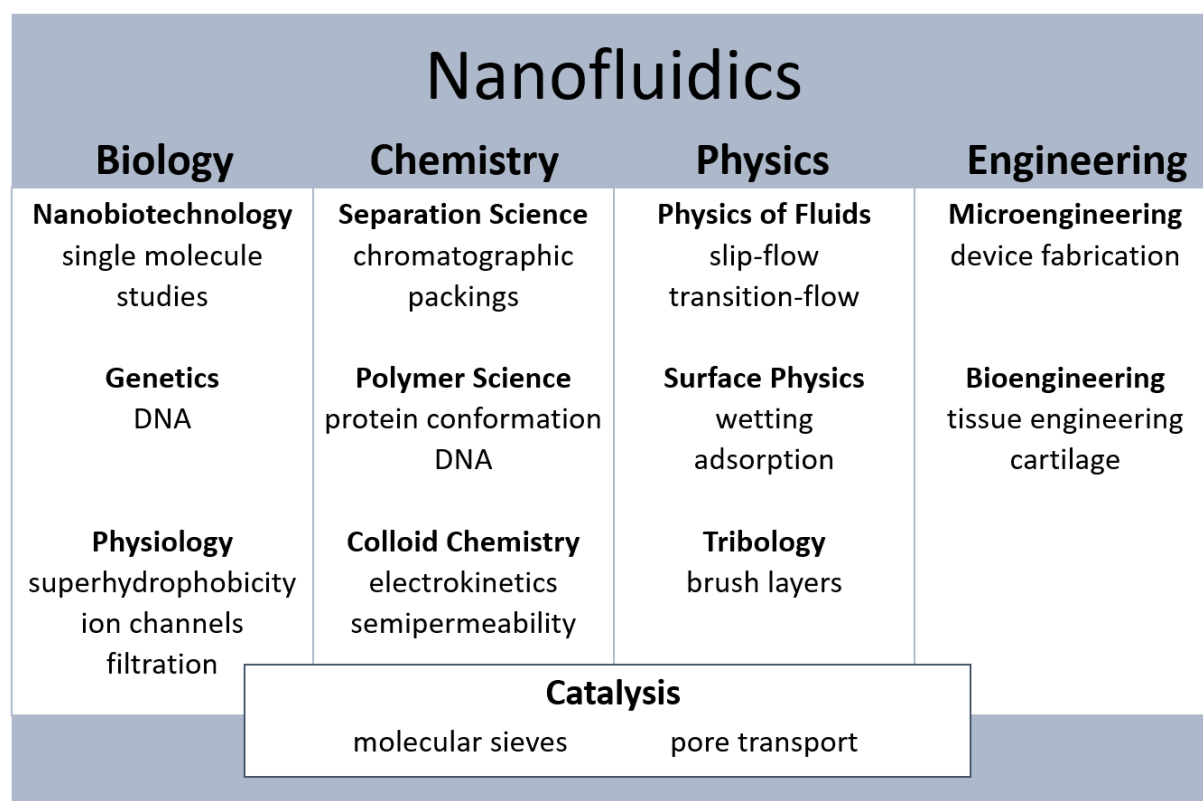| Nanofluidics			
Biology	**Chemistry**	**Physics**	**Engineering**
Nanobiotechnology single molecule studies	**Separation Science** chromatographic packings	**Physics of Fluids** slip-flow transition-flow	**Microengineering** device fabrication
Genetics DNA	**Polymer Science** protein conformation DNA	**Surface Physics** wetting adsorption	**Bioengineering** tissue engineering cartilage
Physiology superhydrophobicity ion channels filtration	**Colloid Chemistry** electrokinetics semipermeability	**Tribology** brush layers	
	Catalysis molecular sieves	pore transport	

Figure 2.1 Overview of the many disciplines covered by the field of nanofluidics. Adapted from[34, 35].

Even though the concepts of nanofluidics have been around for some time, the name nanofluidics only emerged quite recently in conjunction with the rise of microfluidics in the 1990s[34]. At this time, the innovation of new tools during the previous decade, such as atomic force microscopy (AFM), scanning tunneling microscopy (STM) and electron-beam lithography, opened new possibilities for studies on the micro- and nanoscale by allowing for more detailed visualization and manipulation of nanometric

structures. While the transition into smaller size regimes, from micro to nano, can seem as a very natural progression, it is important to keep in mind that physical properties can change dramatically when entering the size range < 100 nm. These changes can be attributed to the huge increase in surface area in comparison to bulk, as well as that the length scales of the confining structures become comparable with characteristic length scales in fluidics, such as Debye length, electronic double layer, and hydrodynamic radius. Hence, the abundance of differences in size-related properties allows for the exploration of new exciting phenomena, but also puts up a challenge since one cannot always rely on classical equations and formulations. With a few decades on its back, multiple studies have already started exploring these new frontiers of changes in liquid properties[36-38], ion current rectification[39, 40], and concentration polarization due to nonlinear transport[41, 42]. Since, as mentioned previously, the field of nanofluidics is very broad, I will not elaborate much on the many aspects of nanofluidic behavior and applications, but will instead refer interested readers to the many reviews covering the topic[31, 32, 43-45]. I will focus on aspects of nanofluidics crucial to the work presented in this thesis, such as the precise control of fluid and mass transport, and the delivery of individual particles and molecules to specific detection/reaction sites in the nanofluidic devices. A few examples where precise flow control has been utilized are in nanoparticle and molecular sieves[46, 47], in single lipid vesicle analysis[48], as well as in stretching of DNA molecules for length determination[49] and DNA mapping[50].

2.2 Nanofabrication

To allow for control of fluids inside a nanofluidic chip, detailed structures in the nanometer scale need to be fabricated. Nanofabrication consists of a multitude of methods to structure materials to nanometric sizes and is generally divided into the two approaches of *bottom up* using self-assembly of molecules or particles, or *top down* using various lithographic techniques or etching. I will here cover the lithographic and etching techniques by which the nanofluidic devices I have used in my thesis were fabricated.

2.2.1 Lithography and Etching

There have been many methods developed to design nano-sized structures, so the list can be made long, but focusing on lithographic techniques, the most prominent are optical lithography[51], electron-beam lithography[21], nanoimprint lithography[52] and scanning probe lithography[53]. In general, lithography is used to create a patterned mask which can be further used for additional processing, such as etching or metal evaporation. The mask is often made from a radiation-sensitive polymer material so that a pattern can be created from irradiation. The exposure (light or electrons) induces a chemical change in the polymer and specific regions (exposed or unexposed) can then be selectively removed with additional chemical processing. The minimum features of the pattern are dictated by the wavelength of the exposing radiation, which is why electron-beam lithography can produce smaller features as compared to traditional optical lithography.

The nanochannels of our nanofluidic chips were fabricated through electron-beam lithography, due to its high precision all the way down to sub-10 nm structures[54, 55]. For larger structures, in the micrometer-scale, the precision of electron-beam lithography was not needed, and the patterns were instead created using optical lithography. The lithography was followed up by reactive ion etching, where channels were etched by exposure to an ionized plasma. For the inlets to the chip, deep reactive ion etching[56] was used to achieve deep and anisotropically etched cylinders.

2.2.2 Nanofluidic device fabrication

Our nanofluidic chips were fabricated from a 4"-silicon (p-type) wafer in the following way (Figure 2.2): (1) Clean the silicon wafer followed by wet oxidation to oxidize the wafer to a depth of 2000 nm. (2) Create alignment marks with electron-beam lithography to assure further structures align properly. (3-1) Make nanochannel structures through electron-beam lithography and reactive ion etching in the presence of Nitrogen trifluoride-flow. (3-2) For chips containing channels with vertical constrictions, add additional spin coating and electron-beam lithography after reactive ion etching to a depth of 30 nm to protect the area of the vertical constriction during the rest of the etching. (4) Define the microchannels by optical lithography followed by reactive ion etching. (5) Make holes though the nanofluidic chip, for supply of liquid, with the same procedure as the microchannels, but followed up with deep reactive ion etching through the silicon layer. (6) Fabricate Au nanoparticles through electron-beam lithography and electron-beam evaporation, for the chips that include lithographic nanoparticles. (7) Clean the substrate and attach a silica lid through fusion

bonding. (8) Cut the 4" wafer with a dicing saw into 16 separate, but identical, chips. This way, a multitude of experiments can be done without variation related to properties of individual batches.

A more detailed description is found in Supplementary Note 1 of **Paper 1**, and Method of **Paper 3** (for details on fabricating the vertical constriction).
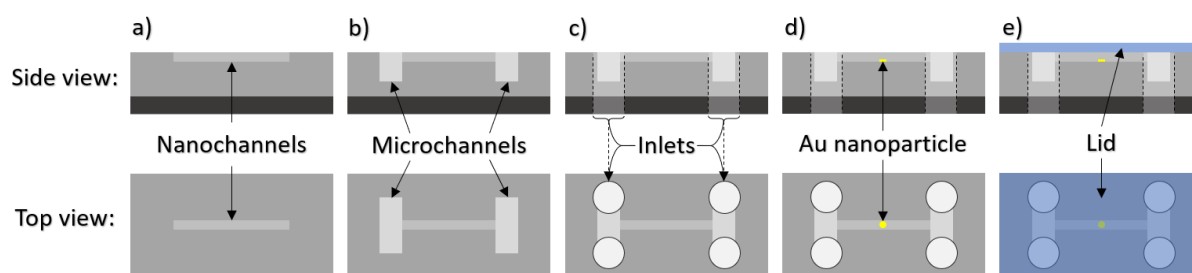

Figure 2.2. Processing steps for fabrication of the nanofluidic devices. (a) Reactive-ion etching of nanochannels into the oxide layer of the Si-chip. (b) Reactive-ion etching of microchannels into the oxide layer of the Si-chip. (c) Deep reactive ion etching of inlets connected to the microchannels. (d) Lithographic fabrication of Au nanoparticles inside the nanochannels, and (e) sealing of the nanofluidic chip with a lid to complete the closed flow system. Adapted with modification from[57].

2.2.3 PSQ bonding – detachable lids

When working with nanofluidics, detachable lids can be very useful to get access to the inside of the nanofluidic system after or in between measurements. In **Paper** 3, we utilized a detachable lid to verify single particle trapping (Figure 2.3) with scanning electron microscopy (SEM). We chose Polysilsesquioxane (PSQ) as our bonding material, since it is known for its excellent aberration resistance, is highly transparent and has a high mechanical modulus[58, 59]. PSQ bonding has been established as a suitable process for nanofluidics with channels as small as 8 nm in height by Gu et. al,[60] and used further in micro and nanofluidic fabrication[61-63]. The process of PSQ bonding is done as follows (see Methods of **Paper 3** for additional details): (1) Clean the silica wafer, with desired nanofluidic structures, and the lid (borosilicate glass) with piranha solution (3:1 mixture of sulfuric acid and hydrogen peroxide). (2) Spin coat freshly prepared PSQ onto the lid and cure it. (3) Expose to O_2 plasma treatment and bring the nanofluidic chip and the PSQ coated lid together to enable the bonding. This bond is sufficiently strong to endure flow pressures inside the device of at least 2 bar and can later be removed by cracking it open from the edge of the chip using a sharp tweezer.
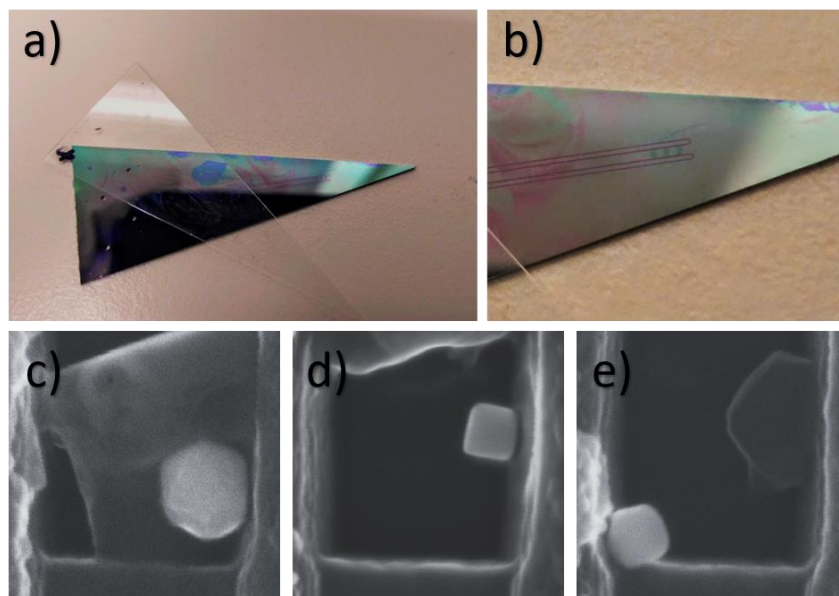
Figure 2.3. Showcase of nanoparticle trapping with detachable PSQ bonded lid. Nanofluidic device with detached lid (a-b) and SEM images of a trapped Au sphere (c), cube (d) and octahedra (e). Adapted with modification from **Paper 3**.

2.3 Nanoparticles

A nanoparticle is usually defined as a particle in the size between 1 and 100 nm[1]. However, the term is often extended to also include sizes up to about 500 nm. Nanoparticles can be formed from a lot of different materials including carbon, metals, ceramics, semiconductors, polymers, or lipids[1]. Biological nanoparticles also exist naturally in our bodies and govern biological functions, such as intercellular communication and protein transfer[10]. While all nanoparticle materials are of scientific interest, in particular metal nanoparticles have shown applicability in a wide variety of fields, such as cancer treatment, solar energy, and catalysis[1]. Two common ways to produce metal nanoparticles are lithographic techniques (*top down*[2]) and/or though colloidal synthesis (*bottom up*)[64]. I will here describe the processes of making and characterizing the nanoparticles handled in this thesis and give examples for how they are utilized in science.

---

[2] Lithographic techniques are mainly *top down* but can also be combined with *bottom up* approaches.

2.3.1   Lithographic nanoparticles

When studying nanoparticles, getting the particles to the place where you can measure their properties and have them stay there can be a struggle. Probably the easiest method to solve this issue is to fabricate the particles in place from the very start. This can be done using various lithographic techniques, such as optical (or electron-beam) lithography, nanosphere lithography and nanoimprint lithography that involve material evaporation to enable particle nucleation and growth on a surface, and lift-off to remove the lithographic masks as the last step[65, 66]. The formation of nanoparticles on a surface is also possible in a less controlled fashion by growing a thin film on a surface by evaporation or sputtering, and thereafter annealing[67]. When evaporating the metal to form nanoparticles, the particles will be amorphous and often with a halo of tiny particles. Therefore, the nanoparticles are generally annealed to form a single- or polycrystalline particle. The thermal treatment also reduces the amount of surrounding tiny particles through Ostwald ripening. An example of this can be seen in Figure 2.4a-b. The structure of lithographically fabricated nanoparticles is generally quite incidental, with mixed surface facets and an abundance of grain boundaries (Figure 2.4c).
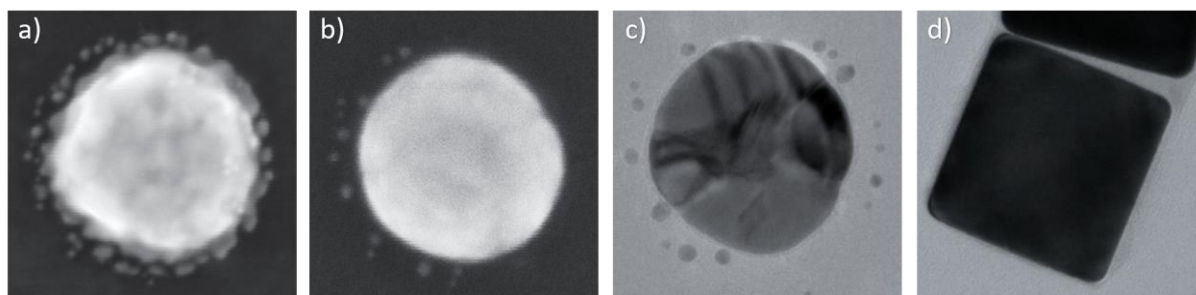

Figure 2.4. SEM images of lithographically fabricated nanodisks before (a) and after (b) annealing. c) TEM image of lithographically fabricated nanodisk after annealing at 550 ° C in N_2 atmosphere for 5 hours. d) TEM image of a colloidal nanocube. Adapted with modification from **Paper 1**[57] **and 3**.

2.3.2   Colloidal nanoparticles

Colloidal nanoparticle synthesis can produce a multitude of highly defined shapes with specific surface facets containing both metals and metal oxides[68-71]. The wealth of particles provides a wide platform for studies on specific structures and their relation to optical, electrical, and catalytic properties. The process of synthesizing colloidal nanoparticles generally consists of reducing a water-soluble metal salt with a reducing

agent to form nanoparticles from the reduced salt. To prevent the particles from aggregation, a stabilization agent is added. Surfactants are often added to provide stabilization and can also be used to control the growth of specific facets to create particles with defined surface facets and specific shapes, such as cubes, rods or octahedra. To tune size and shape, parameters such as temperature, pressure, amount of stirring and reagent concentrations can be varied. The synthesis is traditionally divided into two steps. First, the fast reduction of the metal salt forms seed particles as a base for the particles to grow on. Second, additional reagents are added, possibly in addition to other parameter changes, to achieve conditions resulting in the desired particles. However, there is increasing interest in "single-pot" methods that can improve and simplify synthesis for industrial applications[72, 73]. Colloidal cubes and octahedra with highly defined surface facets were produced for **Paper 3** and an example of the precision of shape-selected colloidal synthesis can be seen in Figure 2.4d.

Ligand exchange

Ligands can play a major role in particle interactions and properties, such as electrostatic charge[74, 75] and catalytic activity[76, 77]. With ligand exchange, one can swap the ligands on the surface of a metal nanoparticle from one type to another one[78]. When producing particles with a more defined structure, some of the common surfactants used to synthesize highly shaped nanoparticles bind strongly to the particle surface. For these cases an intermediate thin metal capping layer can be applied and subsequently etched away in the presence of the desired ligand[79]. For the work presented in this thesis, ligand exchange was used to produce highly defined Au cubes and octahedra capped with citrate or Polyvinylpyrrolidone (PVP) (originally stabilized by Hexadecyltrimethylammonium chloride (CTAC)). This altered the electrostatic charge of the particles from positive to negative and allowed them to be flushed into the nanofluidic system for subsequent trapping (see **Paper 3**).

2.3.3   Fluorescent nanoparticles, lipid vesicles and exosomes

Fluorescent nanoparticles are widely used as a sensing tool for chemical analysis, environmental monitoring, and biological imaging[80]. Additionally, non-fluorescent biological nanoparticles, such as exosomes and lipid vesicles, can be stained by fluorescent probes to monitor their movement or processes with or around them[81]. There exist numerous types of fluorescent nanoparticles and I will here describe the ones I have used in this thesis.

Fluospheres and Polymer dots

Fluospheres and Polymer dots (P-dots) are two types of fluorescent polymer particles designed to be as fluorescently bright as possible. Their structure is different in the sense that fluospheres use a nonfluorescent polymer, polystyrene, to space out highly fluorescent molecules throughout the particles, while P-dots are built up of semiconducting chromophoric polymers[82]. The surfaces of these designed, highly fluorescent nanoparticles are often modified to be used for chemical and biological sensing.

Unilamellar Vesicles

Unilamellar vesicles are spherical vesicles containing aqueous solution that hold together by a single bilayer of amphiphilic lipids[83]. They are used to mimic cells or extracellular vesicles to study biological systems and the lipid membrane can be stained with fluorescent tags for detection using fluorescence; for example, fluorescent lipids or dyes can be bound to the lipid bilayer after the vesicles are formed.

Exosomes

Exosomes are extracellular vesicles, generally in the size range between 30-150 nm in diameter, that are secreted from cells. They have been shown to be important in various biological functions, such as regulation of pathological and physiological diseases, as well as transfer of biomolecules between cells[11]. Therefore, they are of high interest to study as they could act as biomarkers in detecting diseases and assist in developing less invasive diagnostics and treatments. As exosomes are also lipid based, they can be fluorescently stained in similar ways as vesicles for detection. They also carry different nucleic acids and proteins, which can be expressed with fluorescent markers to get a signal that is correlating with the exosome composition.

2.3.4   Characterization of metal nanoparticle

Of the many ways to characterize metal nanoparticles[84] the most prominent are Scanning Electron Microscopy (SEM) and Transmission Electron Microscopy (TEM), due to their output of images with detailed resolution. However, there are several additional techniques used to characterize various other properties, such as catalytic activity, which is discussed in detail in section *4.2.1 Single nanoparticle catalysis*. Below, I go through the characterization techniques used in this thesis.

Electron Microscopy

Imaging by electron microscopy operates by focusing a beam of electrons at the sample of interest. Due to the short wavelength of electrons, images with nanometer or even atomic resolution can be collected. Since electrons also have a short mean free path, a vacuum chamber is generally needed to remove gas molecules that will otherwise scatter the electrons on their way to the sample. By monitoring the scattered light, X-rays, or electrons, or the transmitted electrons, one can collect different information about the sample. With SEM, primarily the backscattered electrons are observed, though secondary electrons can also be monitored. The number of backscattered electrons depends on the molecular weight of the material and thereby provides a material contrast to the recorded image. With TEM the transmitted electrons are recorded and can provide images of high resolution, down to 50 pm[85]. TEM provides a higher resolution, but requires the sample to be very thin (about 100 nm) for the electrons to be transmitted. SEM and TEM provided detailed images of particles and nanofluidic structures in **Paper 1-3**.

Selective Area Electron Diffraction (SAED)

With TEM, the diffracted electrons can also be monitored to create a diffraction pattern that reflects the crystal lattice of the material. The sample material thus acts in analogy to a grating at which the electrons are diffracted and thus scatter with angles related to the distance between the atomic planes in the sample. By examining such diffraction patterns in detail, the distances between atomic planes can be calculated and provide information about the lattice structure and thereby the materials chemical composition.

Energy Dispersive X-ray Spectroscopy (EDS)

When monitoring a sample with electron microscopy, characteristic electrons in the sample will be knocked out by the irradiating beam. The thereby created holes will immediately be filled by electrons in a higher energy state, and the resulting energy loss will induce X-rays that are emitted by the sample. Since the transitions between electronic levels are unique for each element, information about chemical composition can be gathered by examining the energy distribution of the emitted X-rays.

3 Fluorescence and dark field scattering

Early documentation of fluorescent phenomena dates to the 1560s when oxidation of molecules contained in certain types of wood produced a blue infusion[86]. In the early to mid-1800s, several scientists described the same phenomenon for fluorites, chlorophyll, and quinine. Since then, fluorescence has found widespread use in science since it can be tailored to be incorporated in most chemical and biological systems and provide high readout signals in a specified range of wavelengths. Another light-related phenomenon is scattering, and in dark-field scattering, scattered light is monitored to exclusively display highly scattering objects. Both these phenomena have wide use in microscopy applications since they provide a high signal to noise ratio using relatively simple means.

In my thesis I have used fluorescence microscopy to get readout signals in both nanoparticle catalysis (**Paper 1 and 3**) and particle size determination (**Paper 2**), but also utilized dark field microscopy to monitor metal nanoparticles in, for example, nanoparticle trapping (**Paper 3**).

3.1 Fluorescence

To describe fluorescence, I will start with describing light and how it interacts with molecules. Visible light consists of electromagnetic waves with a wavelength that can be detected by the human eye (about 400-700 nm)[87]. Light is also energy, and each light wave contains an energy quantum E related to its wavelength λ according to Eq. 1:

$$E = \frac{hc}{\lambda}. \qquad \text{(Eq. 1)}$$

In this equation h is Planck's constant and c is the speed of light and inputting the wavelengths for visible light results in an energy that spans from about 1.8-3.1 eV. Since light is energy, it can be transformed in various ways, such as being absorbed by a molecule or being generated from an energy decaying process. Fluorescence is one among many such processes.

Molecules are constructed of atoms bound together by chemical bonds. The bonds are facilitated by the atoms positively charged nucleus and negatively charged surrounding electrons. The electrons reside in quantized orbits around the nucleus with energies depending on their angular momentum. For molecules, the configuration of all nuclei results in orbitals in which the individual electrons orbit. Orbitals are also quantized and provide different electronic energy levels which the molecules can reside in. The chemical bonds within the molecules can also contain energy by vibrating and/or rotating. In summary, this results in three main ways that energy within a molecule can be expressed: electronic, vibrational, and rotational. The difference between energy levels in these three modes spans over several orders of magnitudes, electronic being the highest at ~1 eV to vibrational at ~10^{-2} eV and rotational at ~10^{-4} eV[88].

The energy of light can be absorbed by molecules, increasing the energy within the molecule and exciting it to a higher energy state. Since the energy of light is of the same magnitude as the difference between electronic energy levels of molecules, this often results in the excitation of an electron, generally in combination with some vibrational and rotational excitation. After the molecule is excited, several decay processes down to the ground state can occur and among them, fluorescence. The excitation and decay processes can be described in a Jablonksi diagram (Figure 3.1). Starting out, the molecule will reside in its ground state (S_0). After excitation, the energy residing in the vibrational energy levels quickly decays down to its lowest vibrational level by dissipating heat to its surroundings in a process called internal conversion. The energy can then either decay through internal conversion, or fluorescence can occur as radiative decay down to the ground state (but often to an excited vibrational level).
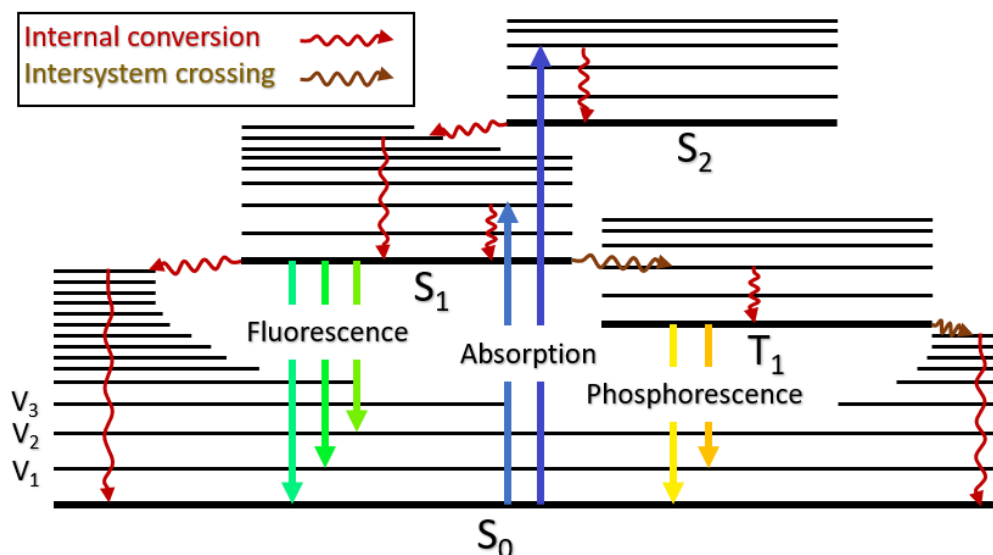
Figure 3.1. Energetic transitions in molecules depicted in a Jablonski diagram. An electron in the ground state (S_0) is excited by absorbed light (blue arrows) and transitions to a higher energy state (S_1 or S_2). Energy is quickly depleted via internal conversion by the vibrational modes (red arrows) down to the bottom of the corresponding electronic state. From there the energy can either continue decaying through internal conversion, be emitted as fluorescence or transition to the triplet state (T_1) through intersystem crossing (brown arrows). From the triplet state, light can also be emitted, but then as phosphorescence (yellow arrows). Alternatively, another intersystem crossing can return the state to S_0 without any radiative process.

The light being emitted as fluorescence generally has a lower energy than the exciting light. The shift in energy is called Stokes' shift and is mainly due to energy loss through internal conversion and that the emission process often decays to an excited vibrational level. However, the surrounding solvent can also affect the decrease in energy, as it can rearrange to align with the altered dipole moment caused by the excitation, which minimizes the energy of the excited state. This is called solvent relaxation and is more prominent for solutions with high polarity as the dipole interactions will then be stronger.

Electrons have an internal angular momentum called spin, which can have one of two directions, up or down. In molecular orbitals, the electrons are generally paired up so that every other electron spin in the opposite direction to minimize the energy. Coupling between the electron spin and the molecular orbitals can split the orbital energy levels into levels depending on how the spins are paired[89]. In the decay process following excitation, the energetic state can sometimes transition into a triplet state (T_1) with different spin multiplicity in a process called intersystem crossing. This process involves a "forbidden" transition which could not take place without orbital coupling. From the triplet state, energy can either decay through emission or to another intersystem crossing back to the singlet state and decay through internal conversion.

If radiative decay occurs from the triplet state it is called phosphorescence and since it again requires a "forbidden" transition, to change the spin back, this happens at a much slower time scale than fluorescence (between ~10^{-3}-10^1 s as opposed to ~10^{-8} s for fluorescence)[90].

3.2   Fluorescent probes

The energy difference between incoming and outgoing light during fluorescence is useful for sensing applications and visualization since it makes it possible to distinguish the incoming exciting light from the outgoing signal using various filters. Consequently, a wide separation between absorption and emission, i.e. a large Stokes' shift is often desired, since it simplifies the light separation. A large Stokes' shift also helps mitigate a decrease in signal through self-quenching, since the outgoing light has a lower probability to be reabsorbed[87].

The brightness of fluorescent probes depends mainly on two parameters: the molar absorption (or extinction coefficient), and the quantum efficiency. The molar absorption dictates how likely light is to be absorbed by the molecule. The parameter varies with the wavelength of the light since it relates to the electronic excitation levels in the molecule. Quantum efficiency instead describes the fraction of absorbed light that is emitted as fluorescence[90].

For a lot of biological and chemical applications, fluorescence is a great tool to visualize interactions between (and inside) cells or chemical reactions[91]. It is also very customizable since fluorescent probes can be tailored to absorb and emit at almost any wavelength[92]. Furthermore, they can be designed to act as reactants in specific chemical reactions[22, 93], or to attach to (or intercalate in) specific biological entities such as DNA[94] or cell membranes[81, 95]. In **Paper 2** several membrane probes were used to stain unilamellar vesicles and exosomes to visualize them with fluorescence microscopy and determine their size.

3.2.1 Fluorescein

Fluorescein is a fluorescent molecule commonly used in fluorescence microscopy[96]. It has a very high quantum efficiency and absorption and emission in the middle of the visible spectrum (Figure 3.2). Fluorescein has a conjugated molecular structure, meaning it has a configuration with alternating single and double bonds. This structure is typical for molecules that are fluorescent in the visible spectral range since it provides π-orbitals with loosely bound electrons that are needed for absorption at these wavelengths[97]. If the conjugation is broken, fluorescein can be rendered non-fluorescent and this type of quenching was used as a read-out signal for the catalytic activity of Au nanoparticles (**Paper 1 and 3**).
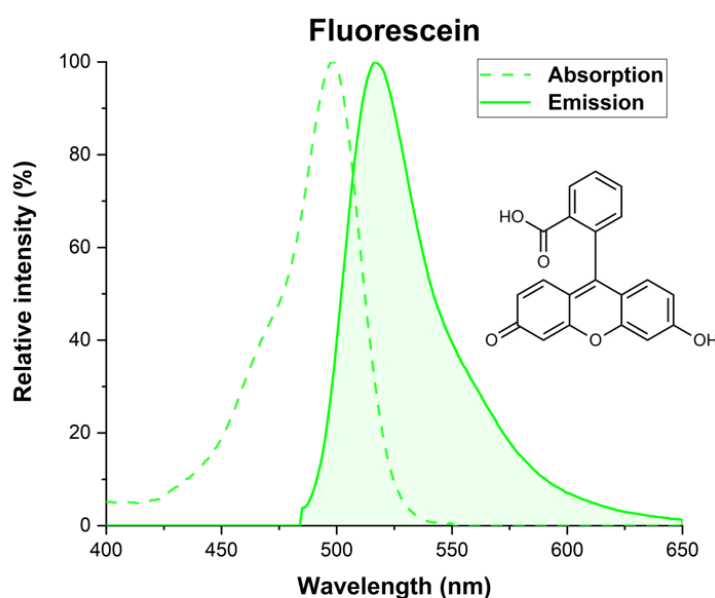

Figure 3.2. Absorption and emission spectra of Fluorescein as well as its molecular structure.

3.3 Fluorescence microscopy

The idea of magnification using optical lenses dates back hundreds of years. The earliest recorded mention of such principles dates back to the 1st century AD[98], although it may have been known about already two thousand years earlier[99]. Today, we have mastered the art of magnification to the point where we are limited by the laws of physics, or namely the diffraction limit of light.

The optical resolution of a microscope is generally given by the Rayleigh criterion[100], which states the minimum distance d between two resolvable points is given by Eq. 2:

$$d = \frac{1.22\lambda}{2n \sin(\theta)} = 0.61\frac{\lambda}{NA}. \qquad \text{(Eq. 2)}$$

Here, n is the index of refraction between the objective and the sample and θ is the half angle of the cone of light that enters the objective. Together they can be combined in the dimensionless parameter numeric aperture given by $NA = n \sin(\theta)$. The numeric aperture describes the range of angles over which the system can emit and collect light. The factor 1.22 comes from calculating the distance between the center and the first minima in the diffraction pattern (Airy disc) from a single point source. For visible light, and a typical numerical aperture of 1.4, this gives a resolution limit of around 200-300 nm depending on the wavelength. However, various methodologies that go beyond the resolution limit and achieve higher resolution have been implemented[101].

In fluorescence microscopy, light of certain wavelengths, overlapping with the absorption spectra (Figure 3.2), are used to excite the fluorophores. Emitted light with higher wavelengths can then be filtered and collected. A typical setup consists of a light source, excitation and emission filters, a dichroic mirror, an objective, and a camera. The light source can either have a broad spectrum, such as an arc discharge lamp, or be monochromatic, such as lasers or LEDs. For the monochromatic light sources, the excitation filter may be excluded since the incoming light is already defined. The dichroic mirror, which selectively reflects or transmits light, and excitation and emission filters are matched with the fluorophore in question to filter incoming and outgoing light. An epi-fluorescence microscope has the sample holder on top of the microscope and images it from below (Figure 3.3). Excitation light is emitted by the light source and passes through the excitation filter where only the specified light is transmitted. The dichroic mirror then reflects it to the objective, which focuses the light on the sample. Emitted light from excited fluorophores is then collected by the objective and sent back through the microscope. When the emitted light hits the dichroic mirror, it is now transmitted because of the dichroic mirror's selectivity towards specific wavelengths. The light is then filtered through an emission filter to minimize noise from backscattering before it reaches the camera and is recorded.
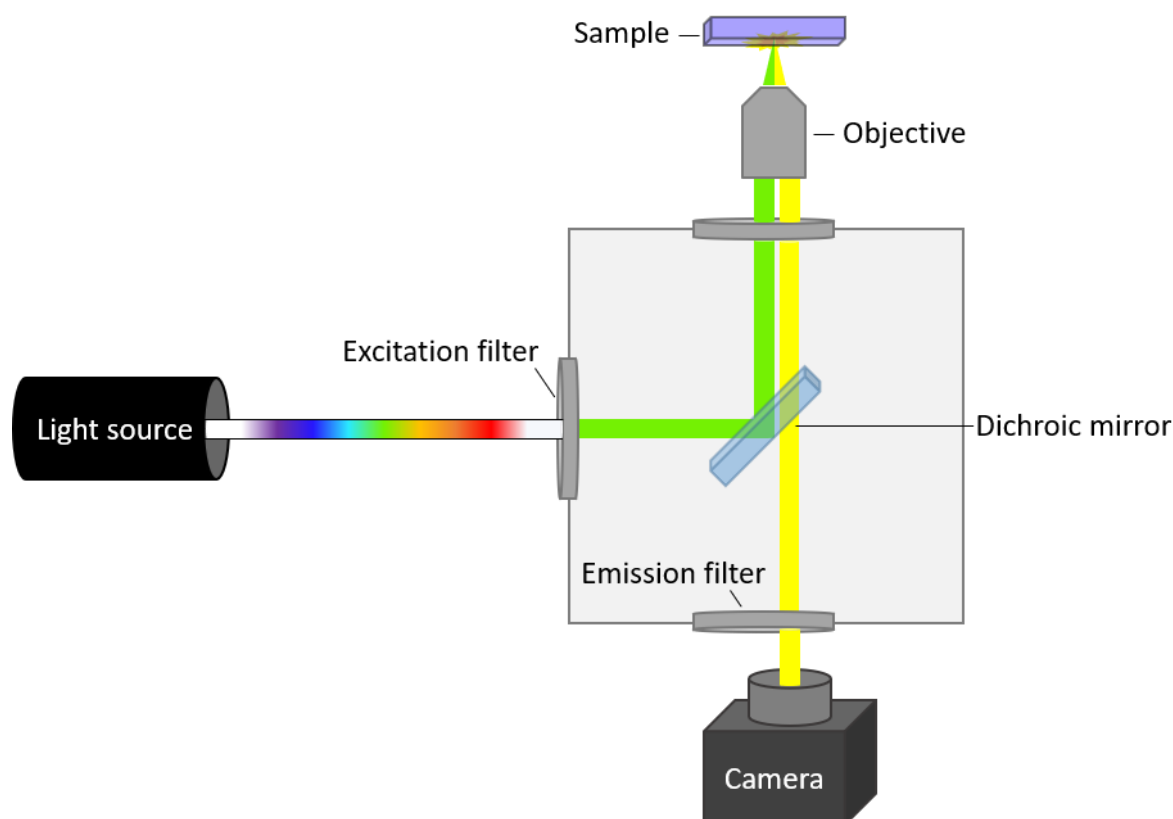
Figure 3.3. A regular epi-fluorescence microscope setup. Light is emitted from a light source and filtered to a specified span of wavelengths by an excitation filter. The light is then reflected on a dichroic mirror and sent through the objective to be focused on the sample. The emitted light from the sample is collected by the objective, transmitted through the dichroic mirror and via an emission filter before it is recorded by the camera.

The signal in fluorescence microscopy scales linearly with the excitation light intensity and a powerful light source is therefore beneficial. However, if fluorophores are exposed to excessive light exposure, they can degrade by cleaving of covalent internal bonds or by non-specific reactions with surrounding molecules in a process called photobleaching[102]. Therefore, there is often a need to find a proper balance between the signal and the amount of photobleaching.

3.4 Dark field microscopy

Scattering is when light interacts with a non-uniformity in its surrounding medium, which forces the light to change direction. These non-uniformities are called scatterers and include anything from particles and bubbles to a rough surface or simply a fluctuation in the density of the medium. Some of the most prominent scatterers are plasmonic metal nanoparticles which scatter very effectively, since their small size

introduces new interactions between their free electrons and light. When the wavelength of the light is longer than the size of the particles, the light waves induce oscillations in the electron cloud and this interaction causes significant scattering and absorption[103]. For plasmonic spheres the absorption and scattering scales exponentially with the radius (r) of the particle according to $I_A \propto r^3$ and $I_S \propto r^6$ respectively. This makes it difficult to detect small spheres (<50 nm) while larger spheres (>100 nm) are very bright[104].

Dark field microscopy can be used to study scatterers. To only record the scattered light, dark field microscopy operates with a condenser lens that sends the exposing light toward the sample at an angle (Figure 3.4a). Light is then collected at a different angle so that only scattered light is recorded. For **Paper 3** dark field microscopy was used to monitor trapping of colloidal metal particles (Figure 3.4b), which were later used in fluorescein reduction experiments monitored with fluorescence (Figure 3.4c).
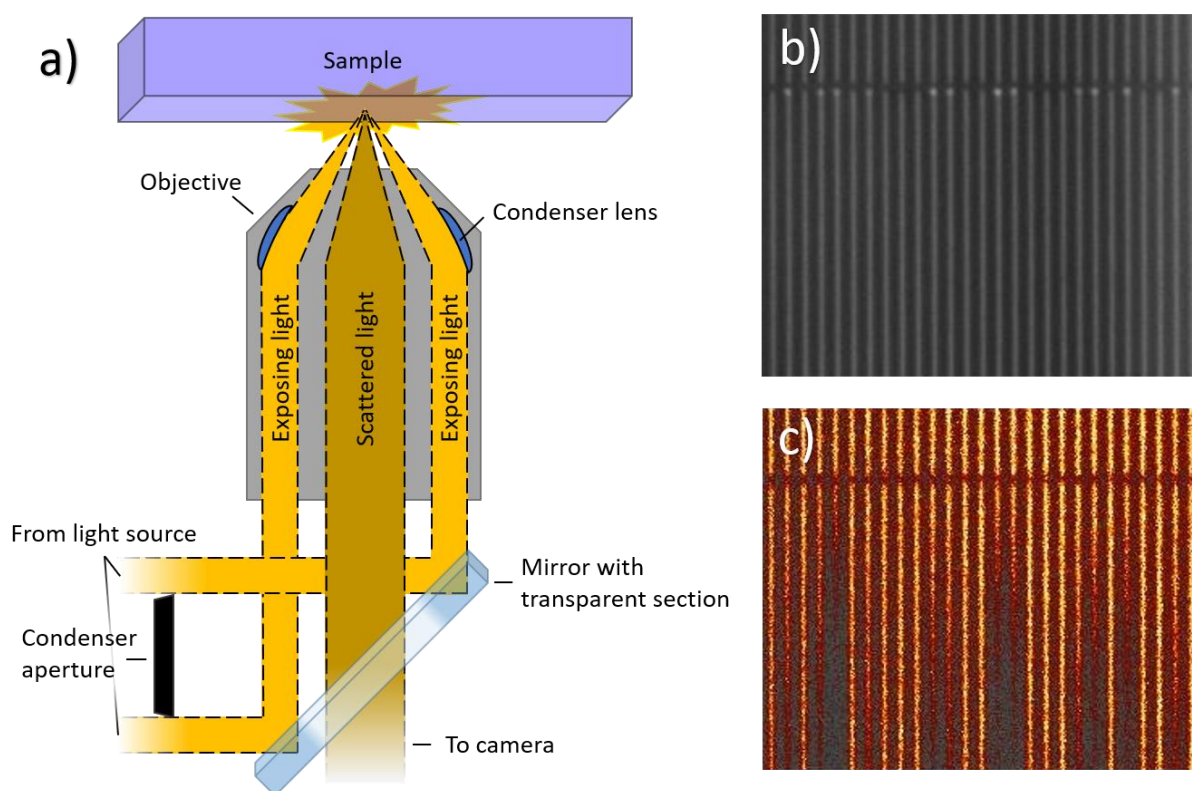

Figure 3.4. The principle behind dark field microscopy and comparison with fluorescence. a) Schematic of how light passes through the dark field objective. Incident light is split up and collected with a condenser lens to reach the sample at an angle. The scattered light is collected at a different angle and transmitted through the centrally transparent mirror to the camera. b) Example of a dark field microscopy image displaying Au nanoparticles in nanochannel traps. c) Example of a fluorescence microscopy image displaying fluorescein reduction on trapped nanoparticles.

4 Catalysis

The word catalysis was first mentioned in 1835 by Jacob Berzelius[105] as a combination of the Greek words **kata**, meaning down, and **lyein**, meaning loosen. He then described the phenomenon as something that influences a chemical reaction without itself being affected. Some 60 years later, Wilhelm Ostwald refined the expression to *"A catalyst is a substance which affects the rate of a chemical reaction without being part of its end product"*[106], which is, more or less, the definition that is used today.

Most people probably think of the catalytic converter in their car when they hear the word catalysis. In the car a catalyst is used in the exhaust pipe to convert toxic gases to harmless ones, but in principle catalysis can be used to increase the rate of any chemical reaction. In our modern-day society, it assists in producing fuels and medicine, and with keeping the air clean.

In this chapter, I will describe the fundamentals of catalysis, in particular heterogeneous catalysis, as well as how I have studied catalytic reactions on single Au nanoparticles.

4.1 The fundamentals of catalysis

A chemical reaction involves transforming one set of chemical substances to another one by breaking and forming chemical bonds. The transformation often entails overcoming one or several energy barriers which, depending on temperature, can be a very slow procedure. In catalysis, the rate of the chemical reaction is increased by a catalyst, which is not itself consumed or altered in the process[107]. Mechanistically, this is possible by the catalyst providing additional pathways along which the reaction can occur under more energetically favorable conditions. In the context of a generic reaction $A + B \rightarrow C$ where two reactants (A and B) react to form the product (C) the catalyst supplies an energetically favourable pathway for the reaction to proceed by and thereby increases the reaction rate. This is illustrated in Figure 4.1 were A and B bind to a catalyst surface and in this way reduce the energy barriers that need to be overcome to transform into C. The energy barrier which must be overcome without a catalyst is defined by the activation energy (E_a). The probability to overcome the barrier can be described by a Boltzmann distribution $P \propto e^{-Ea/k_\beta T}$. If the supplied energy $E = k_\beta T$ is much lower than E_a the probability of the reaction is low and consequently the reaction rate is slow.

Catalysis is often divided into the two categories: homogeneous and heterogeneous catalysis. The categories concern whether the reactants and the catalyst are in the same state of matter (solid, liquid or gas). In homogeneous catalysis, reactants and catalyst are in the same state of matter and typically involves catalysis with organometallic compounds, or acid catalysis[108]. On the border between homogenous and heterogeneous, the category of biocatalysis is sometimes included to cover the numerous reactions catalyzed by enzymes. In heterogeneous catalysis, reactants and catalyst are instead in different states of matter. Most often a solid-state catalyst is used to catalyze liquid or gas phase reactants. Heterogenous catalysis is frequently utilized in chemical and energy related industry applications, to assist in the production of fuels and chemicals. In **Paper 1 and 3**, I have studied heterogeneous catalysis via reduction of fluorescein in the liquid phase on the surface of Au nanoparticles (solid phase). I will therefore elaborate a bit more on the concept of heterogeneous catalysis.
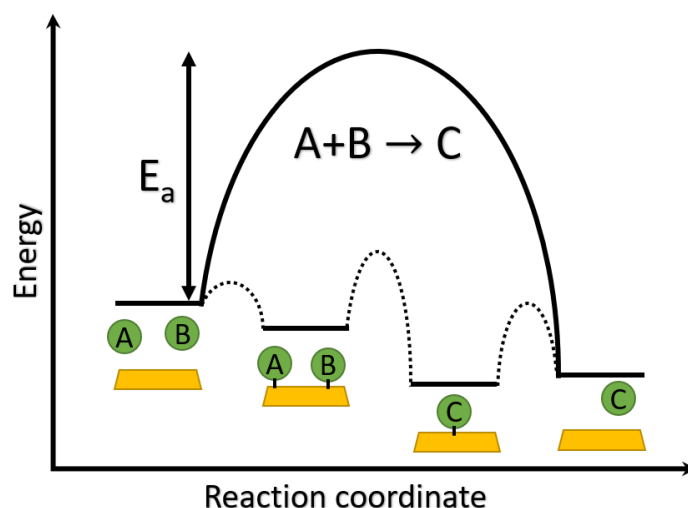
Figure 4.1. An energy diagram displaying the energetically favorable pathway (dotted line) provided by a catalyst. For the generic reaction $A + B \rightarrow C$ the activation energy needed for the uncatalyzed reaction (solid line) would be E_a. With a catalyst present, the reactants A and B can instead adsorb to the catalyst, react into C on the surface, and finally desorb as the reaction product.

An alternate pathway provided by a catalyst is seen as the dotted lines in Figure 4.1. The depicted adsorption of species on a surface is specific for heterogeneous catalysis, but the idea of the altered energy landscape holds true also for homogeneous catalysis. For an effective catalyst, the energy barriers along the new reaction pathway are significantly lower than the barrier without a catalyst, such that less energy is required to drive the reaction[107]. Figure 4.1 also entails typical intermediate steps seen in catalysis. These are (1) reactant adsorption to the catalyst, (2) surface reaction (and dissociation) and (3) desorption of the reaction product(s). After all the three steps, the catalyst is in the same state as before the reaction cycle and ready for new reactants to adsorb. In addition to lowering the energy barriers of the reaction, the adsorption to a surface also keeps the reactants close by each other, which can also contribute to the increase in reactivity. Preferably, the adsorption to the surface is neither too weak, since then the substrate may fail to bind the reactants or not bind them with enough efficiency, nor too strong, which may result in a permanent covering of the surface (poisoning), preventing further reaction to occur. This qualitative concept is called the Sabatier principle after the French chemist Paul Sabatier who first described it[107].

In addition to increasing the rate of the reaction, catalysis can also be used to increase the selectivity, if multiple end products are possible. While the catalyst cannot change the start and end products of a specific reaction, it can increase the rate of certain pathways leading to a specific product. This way, the ratio between end products can be altered, leading to an increased selectivity for the specified reaction product.

4.1.1   Nanoparticles as catalysts

Heterogeneous catalysis is when reactants and catalyst are in different states of matter. Typically, this takes place on the surface of a solid catalyst with liquid or gas reactants. Since the reactants bind to the surface of the catalyst during the reaction cycle, a high surface area is preferable, as it allows for a higher throughput. Nanoparticles supply a large surface area using very little material, since the surface to volume ratio increases dramatically when the particle size is reduced. They are therefore a cheap and sustainable option and are common as catalysts, in particular in the sub-10 nm size range[12, 107, 109]. In addition to an increase in surface to volume ratio, downsizing also increases the curvature of the particles' surfaces, which in turn increases their surface tension, as well as the number of surface atoms with low coordination number. This can make materials such as Au very reactive even though they are essentially inert as a bulk material.

The most common heterogenous catalysts are metal nanoparticles due to their high catalytic activity and chemical stability, as well as the simplicity of their fabrication. The optimum activity is often reached for nanoparticle sizes around 1 nm consisting of only ~20 atoms[110]. The exceptional activity at this nanoparticle size is usually attributed to the increased fraction of low coordinated surface atoms, such as edges and corners, which have shown to be highly active[111, 112]. For larger nanoparticles, differences in surface facets have shown to be important, as well as the presence of defects or grain boundaries which also alter the surface energy landscape and provide additional low coordinated surface atoms. Nanoparticles are often fixed on a substrate and the substrate material can also play an important role for the activity as the tension between particle and substrate can alter the particle structure. The substrate can also facilitate the reaction, for example by acting as a reservoir of reactant species, for example oxygen atoms. The activity of the catalyst is generally expressed in terms of turnover frequency (ToF) per active site[113]. The ToF describes how many reaction cycles that occur at an active surface site per unit time. An active site is a small area on the catalyst where the reaction can occur, and it is used to distinguish between differently coordinated surface sites, such as corners, edges, and defects. Although the active site often occupies more space than single surface atoms, the number of active sites generally scales linearly with the number of surface atoms. Therefore, the ToF is sometimes given per surface atom when no detailed specification or knowledge of the occupied area of the active site is available.

In addition to experimental evidence for differences in catalytic activity between different surface facets, theoretical modelling using density functional theory (DFT)[114, 115] is widely used to validate experimental findings and to rationally design catalyst

materials. The constant increase in computational power has made it feasible to simulate complete nanoparticles up to sizes of 5 nm using DFT[116, 117]. These kinds of simulations make it possible to link experimental results with theoretical models to make more substantiated claims based on combined experimental and theoretical results.

4.2 Methods to measure nanoparticle catalysis

Studies regarding nanoparticles in catalysis were published as early as 1941[118], with palladium and platinum nanoparticles catalyzing a hydrogenation reaction. A later advance of the field was made by Haruta in 1987 when he discovered that activity for the oxidation reaction of CO to CO_2 was increased for Au particles smaller than 5 nm[119]. Since then, the main focus within nanoparticle catalysis has been towards the improved catalytic performance of smaller nanoparticles (~1-10 nm), though with some exceptions, such as interaction with plasmon resonance and the generation of hot electrons, where larger nanoparticles are preferred[120].

In the 60s and 70s, although it was already possible to study catalysis from nanoparticles, the studied catalysts were commonly replaced by simpler "models", such as single crystalline surfaces to more easily investigate them using so-called surface science techniques[121]. With advances in related instrumentation, surface science took a main role in catalysis, with methods, such as Auger electron spectroscopy (AES) and X-ray photoelectron spectroscopy (XPS), that could be used to probe the catalyst surface, and low energy electron diffraction (LEED) to also measure its adsorbed molecules. Adjointly, reactants and products from the catalysis could be monitored with a quadropole mass spectrometer or by gas chromatography. With further advances in surface characterization techniques, such as scanning tunneling microscopy (STM), atomic force microscopy (AFM) and electron microscopy techniques (SEM and TEM), the visualization of surfaces of nanoparticles down to atomic resolution has increased our insight tremendously since the days of classical surface science. Together with techniques such as X-ray diffraction (XRD) to determine crystallinity, infrared and Raman spectroscopy to monitor adsorbed species, as well as mass spectrometry to evaluate the consumption of reactants and/or formation of products, a lot of information can be gathered from these systems that were previously nearly impossible to observe.

Nanoparticle catalysis measurements have traditionally been done on ensembles of particles where the differences between individual particles are averaged out. With an

increasingly detailed view onto nanoparticle catalysis, understanding particle heterogeneity has become exceedingly important, as individual nanoparticles may exhibit different activity and selectivity. It has therefore become critical to examine single nanoparticles to increase our knowledge of nanoparticle catalysis even further.

4.2.1 Single nanoparticle catalysis

In response to the issue of ensemble averaging in batch measurements, methods capable of resolving relevant properties of single catalyst particles, such as size, crystallinity, surface bound molecules or catalytic activity, have emerged. Since nanoparticles are small, they interact weakly with any radiation used to probe them and produce a very low number of reaction products individually. High sensitivity is therefore crucial for any single particle measurement to resolve the particles individual properties. In Table 1, an overview of selected relevant single particle techniques is presented together with a description of how they operate, and their respective limitations. The properties measured by these methods can be categorized into three main readouts from single nanoparticles techniques: (1) reaction rate, (2) surface species and (3) shape, size, oxidation state and/or chemical composition.

(1) First, we have reaction rate, which can be measured via single-molecule fluorescence microscopy (SMFM)[122-125] through detection of single molecules, scan electrochemical microscopy (SECM)[126] by evaluation of electric current produced from the reaction, or parallelized nanofluidic fluorescence microscopy[57] by monitoring the difference in fluorescence downstream of the catalyst[3]. (2) Second, the molecules on the catalyst surface can be measured via surface- or tip-enhanced Raman scattering (SERS/TERS)[127-130] through the enhanced Raman signal from the catalyst, synchrotron-radiation-based infrared nanospectroscopy (SINS)[131], or surface-enhanced infrared absorption spectroscopy (SEIRAS)**[132]**, which probe molecular vibrations in the IR spectra. (3) Third, nanoparticle shape, size, oxidation state and/or chemical composition can be determined with plasmonic nanospectroscopy[133-135] by evaluation of the spectral shift in plasmonic resonance, X-ray microscopy[136] that probes the oxidation state and coordination environment, or environmental transmission electron microscopy (ETEM)[137] that provides high resolution images during catalytic reaction. In addition to measuring different properties of the catalyst, the different methods described above often come with restrictive limitations, such as the need of fluorescent reactants or products, the necessity of plasmonically active nanoparticles, or the inability to supply activity information.

---

[3] The method I have presented in **Paper 1 and 3**.

Table 1. Overview of methods for measuring single nanoparticle catalysis and their respective limitations. Adapted with modification from[35].

Method	Principle	Readout	Limitations
Single-molecule Fluorescence Microscopy (SMFM)[122-125]	Detection of single fluorescent molecules turning on or off at the catalyst surface	Residence times and reaction rate	Needs fluorescent read out, low reactant concentration and/or low reaction rate
Scan Electrochemical Microscopy (SECM)[126]	Measurement of the electric current produced from electro-chemical reaction occurring on a catalyst particle	Reaction rate	Limited to liquid phase. Tip crash can damage the sample, and separate electrode needed for each experiment
Parallelized Nanofluidic Fluorescence Microscopy[57]	Detection of fluorescence change downstream of catalyst nanoparticle	Reaction rate, flow profile	Requires fluorescent readout and high reaction rate
Surface-enhanced Raman Scattering (SERS)[127, 128]	Raman spectroscopy with surface enhancement from plasmonic catalyst	Molecules on catalyst particle surface	Requires plasmonic catalyst. Weak signal enhancement on single crystal surfaces
Tip-enhanced Raman Spectroscopy (TERS)[129, 130]	AFM in combination with a probe light beam to detect Raman shift induced by molecular vibrations in the IR range	Molecules on catalyst particle surface	Requires plasmonic catalyst. Enhancement from tips may vary and hamper reproducibility. Known tip enhancement is therefore crucial
Synchrotron-radiation-based Infrared Nanospectroscopy (SINS)[131]	AFM in combination with synchrotron IR light scattering that probes molecular vibrations	Molecules on catalyst particle surface	Needs synchrotron infrastructure. Weak signal due to low scattering cross section
Surface-enhanced Infrared Absorption Spectroscopy (SEIRAS)[132]	Detection of molecular vibrations in the IR range via surface enhancement and spectroscopy	Molecules on catalyst particle surface	Requires plasmonic catalyst and provide low signals. Not yet established for catalysis.
Plasmonic Nanospectroscopy[133, 134]	Monitoring of the spectral shift in plasmon resonance and relating it to chemical or physical property changes in the catalyst particle or its local environment	Nanoparticle size, shape, oxidation state and surrounding environment	Supplies no activity information and requires plasmonic particles. Readout can be due to several different effects and needs to be interpreted carefully
X-Ray Microscopy[136]	Evaluation of X-rays to detect changes in the oxidation state and coordination of catalyst atoms	Oxidation state and coordination of catalyst particle	Supplies no activity information and requires synchrotron infrastructure. High intensity X-rays may damage the catalyst
Environmental Transmission Electron Microscopy (ETEM)[137]	TEM with a confined high pressure region close to the sample	Structure of catalyst particle	No activity information, limited field of view and complex infrastructure. Catalyst may be damaged by high energy electrons

4.3 Parallelized nanofluidic fluorescence microscopy

Parallelized nanofluidic fluorescence microscopy is a method that I have developed during my doctoral studies (**Paper 1 and 3**). It provides a complementary platform to compensate for some of the limitations of the other single particle catalysis techniques.

4.3.1 Reduction of fluorescein on nanoparticles

Parallelized nanofluidic fluorescence microscopy[57] utilizes the fast reduction of fluorescein by sodium borohydride on the surface of Au nanoparticles as a model reaction. By determining the fraction of reduced fluorescein molecules downstream of single nanoparticles in individual nanochannels (Figure 3.4b-c), the catalytic activity can be determined for each single particle. Fluorescein reduction on nanoparticles has previously been studies with both absorption spectroscopy[138] and fluorescence spectroscopy[139] and is useful both due to the reaction's relatively high rate and the prominent change in absorption and fluorescence as its result.

Fluorescein reduction has also been studied extensively in electrochemistry by R. G. Compton, et al.[140-145] where it has been shown to reduce through an electrochemical chemical electrochemical (ECE), or disproportion mechanism depending on illumination and/or pH of the reactant solution. On the surface of nanoparticles, it has been understood as an electrochemical process, where the nanoparticle acts as an electron relay between the sodium borohydride and the fluorescein[138, 139]. The mechanisms governing the reduction at high fluorescein concentration is discussed further in **Paper 3**, where the Au nanoparticles display diminished catalytic activity at high fluorescein concentrations followed by a transition into the mass transport limited regime as the concentration decreases.

4.3.2 Amplex red reduction

Another fluorophore that has been widely used in single nanoparticle catalysis is Amplex red[146, 147] that can be reduced by hydrogen peroxide. It has shown promise in parallelized nanofluidic fluorescence microscopy[57], even though the reaction rate is significantly lower than that of the fluorescein reduction reaction. When measuring Amplex red reduction through fluorescence, it is particularly important to be mindful of the amount of light exposure, since Amplex red reduction has shown to be auto-catalyzed by light[148]. However, with clever implementation, its photochemical properties can instead be used to an advantage in, for example, photocatalysis[149].

5 Size determination by particle tracking

The importance of particle size has been known for a long time. Already in ancient Egypt, sieves were used to evaluate grain size and grade the harvests[150]. Today, we have developed techniques that can characterize and sometimes even sort particles of sizes on the nanometer scale. Particle size analysis is applied in many different fields and industries, such as cosmetics, food, or pharmaceutical industry[1]. In the last decades, several techniques to measure particle diffusion from light scattering or fluorescence have made it possible to characterize the size of micro- and nanoparticles with high precision and high throughput.

In **Paper 2** in this thesis, the method Nano-SMF is presented, which measures particle size and intensity in multiple fluorescence colors for particles in the size range 20-200 nm in diameter. The combined size and intensity information gives insight in the functions of exosomes and helps increase our understanding of extracellular interactions. I will in this chapter describe how size can be extracted from the Brownian motion of spherical particles and describe the method Nano-SMF in the context of other particle size analysis techniques.

5.1 Brownian motion

"Observe what happens when sunbeams are admitted into a building and shed light on its shadowy places. You will see a multitude of tiny particles mingling in a multitude of ways in the empty space within the light of the beam, as though contending in everlasting conflict, rushing into battle rank upon rank with never a moment's pause in a rapid sequence of unions and dis-unions… their dancing is an actual indication of underlying movements of matter that are hidden from our sight... It originates with the atoms which move of themselves. Then those small compound bodies that are least removed from the impetus of the atoms are set in motion by the impact of their invisible blows and in turn cannon against slightly larger bodies. So the movement mounts up from the atoms and gradually emerges to the level of our senses so that those bodies are in motion that we see in sunbeams, moved by blows that remain invisible."

The quote above is part of a scientific poem *"On the Nature of Things"* by the Roman philosopher-poet Lucretius in 60 BC[151]. It quite brilliantly describes the essence of Brownian dynamics; albeit with an incorrect example since the mingling motion of dust particles is mainly caused by air currents.

It would take about 1800 years until Brownian motion was observed and described correctly by Robert Brown in 1827[152]. Brownian motion consists of random motion of particles suspended in a gas or a liquid. In the early 1900s it was described in the context of physics by, among others, Albert Einstein. He found that the diffusion D of a particle, would depend on its mobility μ and the temperature T according to:

$$D = \mu \cdot k_\beta \cdot T, \qquad \text{(Eq. 3)}$$

where k_β is Boltzmann's constant. In a liquid with laminar flow, i.e. low Reynolds number, the mobility can be described by the inverse of the drag coefficient ζ. For a spherical particle with the radius r the drag coefficient is given by Stokes' law as $\zeta = 6\pi \cdot \eta \cdot r$, where η is the liquids viscosity. Combining Stokes' law with the Einstein relation (Eq. 3) gives the Stokes-Einstein equation[153]

$$D = \frac{k_\beta \cdot T}{6\pi \cdot \eta \cdot r}, \qquad \text{(Eq. 4)}$$

which describes the diffusion of a spherical particle in laminar flow.

5.1.1　Size determination from Brownian motion

Determining the properties of particles is essential for a range of fields, such as pollution control, electronics, and biomedicine[154]. Among particle properties, size is one of the most important to characterize since it often influences the particle behavior in various ways, for example by affecting particle agglomeration or cellular uptake. There are numerous bulk techniques to determine particle size, such as dynamic light scattering (DLS)[155], tunable resistive pulse sensing (TRPS)[156], or differential centrifugal sedimentation (DCS)[157]. Since nanoparticles are often heterogeneous, single particle resolution, with more detail on particle size distribution, is often wanted. To this end, it is possible to attach the particles to a surface and measure the size with atomic force microscopy (AFM) or electron microscopy (SEM/TEM). These techniques do not allow for very high throughput, which can instead be achieved with different particle flow techniques, such as nanoparticle tracking analysis (NTA)[27] or flow cytometry (FC)[158]. NTA determines the size of the particles by tracking the movement of individual particles, via scattering or fluorescence microscopy, in three dimensions to determine their diffusion coefficient. The hydrodynamic radius for each particle can then be determined via the Stokes-Einstein equation (Eq. 4). Since the particle trajectory is tracked for particles moving in three dimensions, the particles can move in and out of the focal plane, which produces artefacts in the collected intensity and limits simultaneous evaluation of particle size and intensity[159]. One way to improve on this aspect is by tethering the particles to a supported lipid bilayer and investigate the diffusion in only two dimensions via two-dimensional flow nanometry[160]. This way the focus is maintained over a longer time which allows for longer trajectories with more stable intensity. A step further in the same direction is Nano-SMF (SMF; size and multiplexed fluorescence), that we have developed on the basis of nano flow cytomery[48], where the particles are restricted to one dimension by confinement in nanochannels (**Paper 2**). This way, the diffusion in the one remaining dimension can be evaluated and the particles are retained in focus throughout the particle trajectories without the need of tethering.

5.2　Nano-SMF

In **Paper 2**, a method to measure the size of nanometer sized vesicles called Nano-SMF is presented. In Nano-SMF fluorescent particles are flushed slowly through an array of nanochannels (Figure 5.1), so that the primary motion exerted by the particles is from diffusion (Brownian motion). By tracking the particles and subtracting the mean

speed, from a slow driving flow, single particle trajectories can be collected (Figure 5.1d). Similar to how the size is determined with NTA, the diffusion from these trajectories can be calculated through mean square displacement and the size can then be determined with the use of the Stokes'-Einstein equation (Eq. 4). However, since the particle movements are constricted by the nanochannels, the diffusion needs to be corrected by a hinderance factor depending on the particle size and the nanochannel dimensions. Analysis of the particle trajectories yields size and fluorescence intensity for all particles flushed through the field of view, which generally amounts to 10^3-10^4 particles recorded during 5 minutes of acquisition. For a system of nanochannels with square shaped cross-section of 300x300 nm^2, particle sizes between 20-200 nm can be determined. While no tethering is needed, the channel walls are often coated by a supported lipid bilayer[161] to decrease the risk of nanoparticles sticking to the channel walls and clogging of the nanochannels.
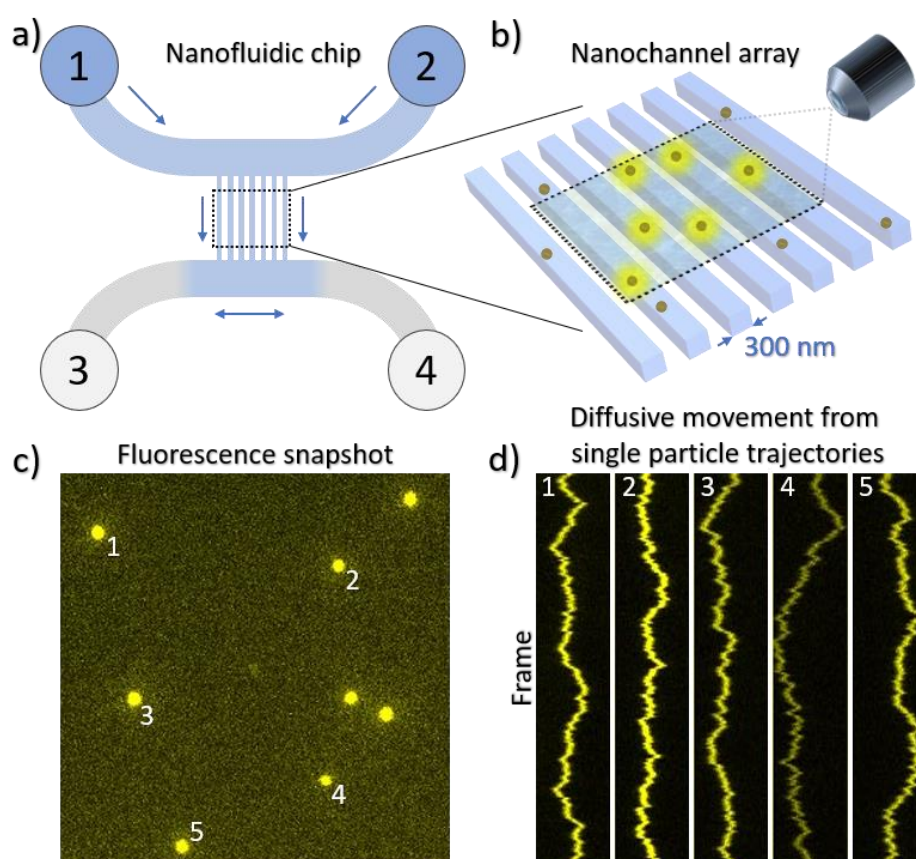
Figure 5.1. Schematic of a Nano-SMF device. a) Layout of the nanofluidic chip with four inlets connected by two microchannels leading to an array of 100 nanochannels. b) Illustration of parallel nanochannels containing fluorescent particles. c) Snapshot of 100 nm fluorescent polystyrene beads flowing through the nanochannel array. d) Single particle trajectories during 200 video frames collected from the numbered particles in c. Adapted with modification from **Paper 2**.

5.2.1 Hinderance factor

Particles diffusing in a narrow channel will experience hydrodynamic coupling to the channel walls. The walls limit the particle movement and thereby decrease the diffusion of the restricted particle as compared to a freely diffusing particle. One way to account for this decrease in diffusion is by introducing a hinderance factor H which rescales the diffusion coefficient according to $D_{constricted} = H \cdot D_{free}$. H depends on both the channel geometry and size, as well as the particle size[162]. In a nanochannel with the cross-section of a square, H has been determined through the center-line approximation to be

$$H = \frac{1 - 2.105 \cdot \lambda + 2.0865 \cdot \lambda^3 - 1.7068 \cdot \lambda^5 + 0.72603 \cdot \lambda^6}{1 - 0.666 \cdot \lambda^2 - 0.20217 \cdot \lambda^5}. \qquad \text{(Eq. 5)}$$

The parameter λ is here given by $\lambda = \sqrt{\pi} \cdot r / a$, where r is the particles hydrodynamic radius and a is the side length of the nanochannel cross-section[163]. This relation can be inverted to generate the particle radius from the constricted diffusion recorded in the nanochannels and is used to determine particle sizes with Nano-SMF.

5.2.2 Flow speed and exposure time

Nano-SMF operates under conditions where particle movement is mainly dictated by diffusion. It is therefore restricted to relatively low flow speeds (<~20 µm/s). If higher flow speeds are used, the diffusion part of the movement is distorted, and the particle size is underestimated (Figure 5.2a).

To calculate particle diffusivity, the stochastic component of the motion is extracted from the mean square displacement between consecutive frames. When doing this, the exposure time needs to be considered. The particle position in each frame will be determined by the particle position throughout the exposure time, resulting in a motion blur on the recorded intensity distribution[164]. To account for this, the acquired diffusion needs to be adjusted via multiplication by a correction factor ε given by

$$\varepsilon = \frac{3 \cdot \Delta t}{3 \cdot \Delta t - \Delta t_0}, \qquad \text{(Eq. 6)}$$

where Δt is the time between frames and Δt_0 is the exposure time.

Even if the motion blur is accounted for, the diffusivity will be overestimated if too long exposure times are used (Figure 5.2b). This is probably related to how the intensity profile collected over an extended time will be elongated and not represented

by a Gaussian profile. The elongation will result in a deviation in the determined particle position, compared to the mean particle position during the exposure time. That deviation will in turn result in an error in the size and could be responsible for the underestimation seen at longer exposure times.
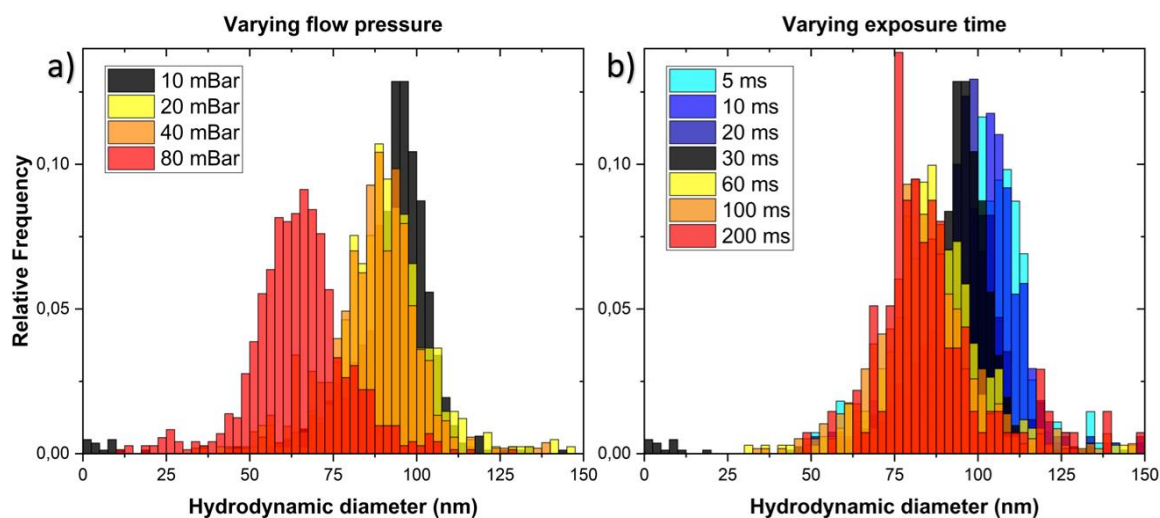

Figure 5.2. Size distributions for 100 nm polystyrene beads and how the determination of their size varies with (a) increasing flow pressure (i.e. flow speed) or (b) increasing exposure time. Adapted with modification from **Paper 2**.

5.2.3   Colocalization - detecting subpopulations

Nano-SMF can also record particle trajectories in multiple color channels by sequentially switching the excitation light and using a multi bandpass filter. This way, fluorescence in multiple colors can be collected for a multitude of particles and size can be determined. Additionally, the particle trajectories can be co-localized by examining whether the trajectories collected in the different color channels follow each other closely, both in time and space. With information regarding size, and fluorescence intensity in multiple colors, subpopulations regarding size and interactions with multiple fluorescence probes can be investigated with just one measurement.

6 Original Work

The major findings obtained in this work are enclosed in the three papers appended to the thesis. However, additional relevant findings, which need more research before clear conclusions can be drawn, were also produced. In this chapter, I will summarize the main findings in the appended papers and expand upon some of the additional findings acquired during my doctoral studies.

6.1 Summary of results

In this section, the main findings of the appended papers are summarized.

6.1.1 Paper 1

Heterogeneity in catalytic activity among nanoparticles is prevalent, and studies of catalysis on the single particle level is needed to fully understand how to optimize the use of nanoparticles in catalysis. There exist multiple techniques to study single nanoparticle catalysis, but all of them have limitations, such as requiring low reaction concentrations and/or reaction rate, or having low throughput. In **Paper 1**, we wanted to utilize controlled flow in a nanofluidic system, which keeps the liquid in the focus of the microscope, to measure catalysis on single nanoparticles at high throughput and reaction rates, and compensate for some of the limitations of established methods. For this purpose, we fabricated 35 lithographic Au nanodisks with diameters ranging from 64 to 128 nm in diameter, each one situated in its own channel, in an array of parallel nanochannels. Using the reduction of fluorescein by sodium borohydride as a model reaction, we could determine the fluorescence downstream of the nanoparticles and estimate their individual turnover frequency (ToF) (Figure 6.1). This gave insight into how the catalytic activity transitions from a reaction limited regime to a mass transport limited regime as the fluorescein concentration decreases, and that the transition depends on particle size. The maximum ToF reached for each particle did however not depend on particle size, but a large heterogeneity was observed between individual particles. Detailed characterization of particle structure with TEM of analogous particles on a TEM membrane revealed a spread in the number of grain boundaries, which could be the reason for the differences in catalytic activity.

In contrast to other single particle catalysis methods, parallelized nanofluidic fluorescence microscopy can operate at relatively high reactant concentration and reaction rate, in the range of relevant industrial applications. Furthermore, the separation of the particles in individual parallel channels ensures identical reaction conditions for tens of single nanoparticles that could be monitored simultaneously. In the future, the method can be combined with other single nanoparticle techniques to provide the capability of measurements in a broader concentration range.
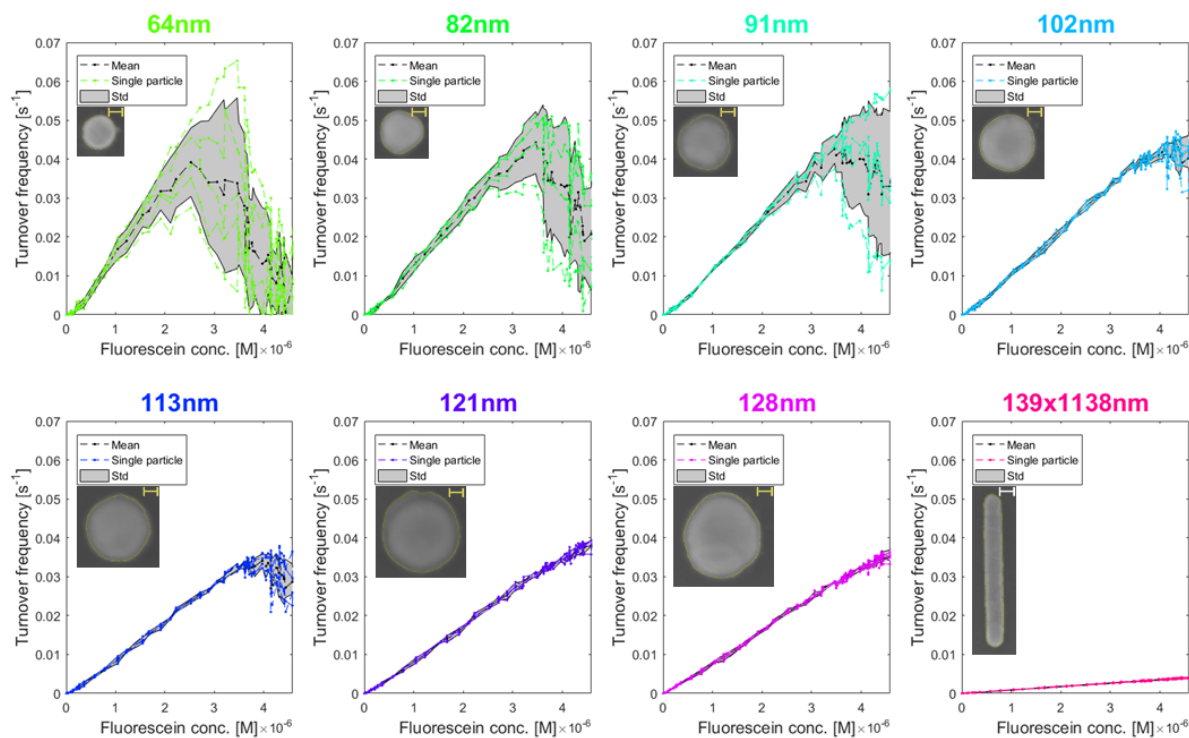
Figure 6.1. Summary of single particle-specific and mean turnover frequencies (ToFs) for all 32 particles studied in parallel in a single experiment at different nominal incoming fluorescein concentrations. The titles display the nominal particle diameters, and the insets show SEM images of corresponding particle analogues taken after cleaning on an open surface. The scale bars are 20 nm in all insets except for the 139 x 1138 nm patch where it is 100 nm. Black and colored lines display mean and individual particle ToFs, respectively, and the gray shaded areas depict the standard deviation. The fluorescein concentration was systematically varied between 0 and 4.6 µM and the borohydride concentration was kept constant at 50 mM.

6.1.2 Paper 2

It is difficult to determine the size of biological particles below 300 nm in diameter. In **Paper 2**, we present a newly developed method we call Nano-SMF (SMF; size and multiplexed fluorescence). Nano-SMF relies on determining the size of particles of sizes 20-200 nm in diameter by detecting the one-dimensional Brownian motion and at the same time recording their fluorescence intensity in multiple colors. This is done by confining the particles in nanochannels (with cross section of 300x300 nm²) and flowing them slowly through the nanochannels so that their movement is dominated by Brownian motion. The confinement retains the particles in the focus of the microscope throughout their trajectory and thereby provides a good signal to accurately determine both particle positions and intensities. With the use of the Stokes-Einstein equation in combination with a hindrance factor to account for the constricted diffusion in the nanochannels, the particle sizes can be determined solely from their

1D diffusion. Thereby, the method provides uncoupled size and intensity data from which conclusions regarding size and intensity scaling can be drawn. The array of nanochannels also spaces out the particles, which allows for analyzing samples with a wide range of particle intensities; thereby providing detailed size distributions for polydisperse samples (regarding both size and intensity) as compared to NTA (Figure 6.2). Nano-SMF is not restricted to fluorescence, but can be applied with other techniques, such as dark field microscopy which is showcased using spherical Au nanoparticles of 60 and 100 nm in diameter. The minimal size that can be determined is limited by the signal to noise ratio and for highly fluorescent P-dots sizes down to 20 nm in diameter can be resolved.
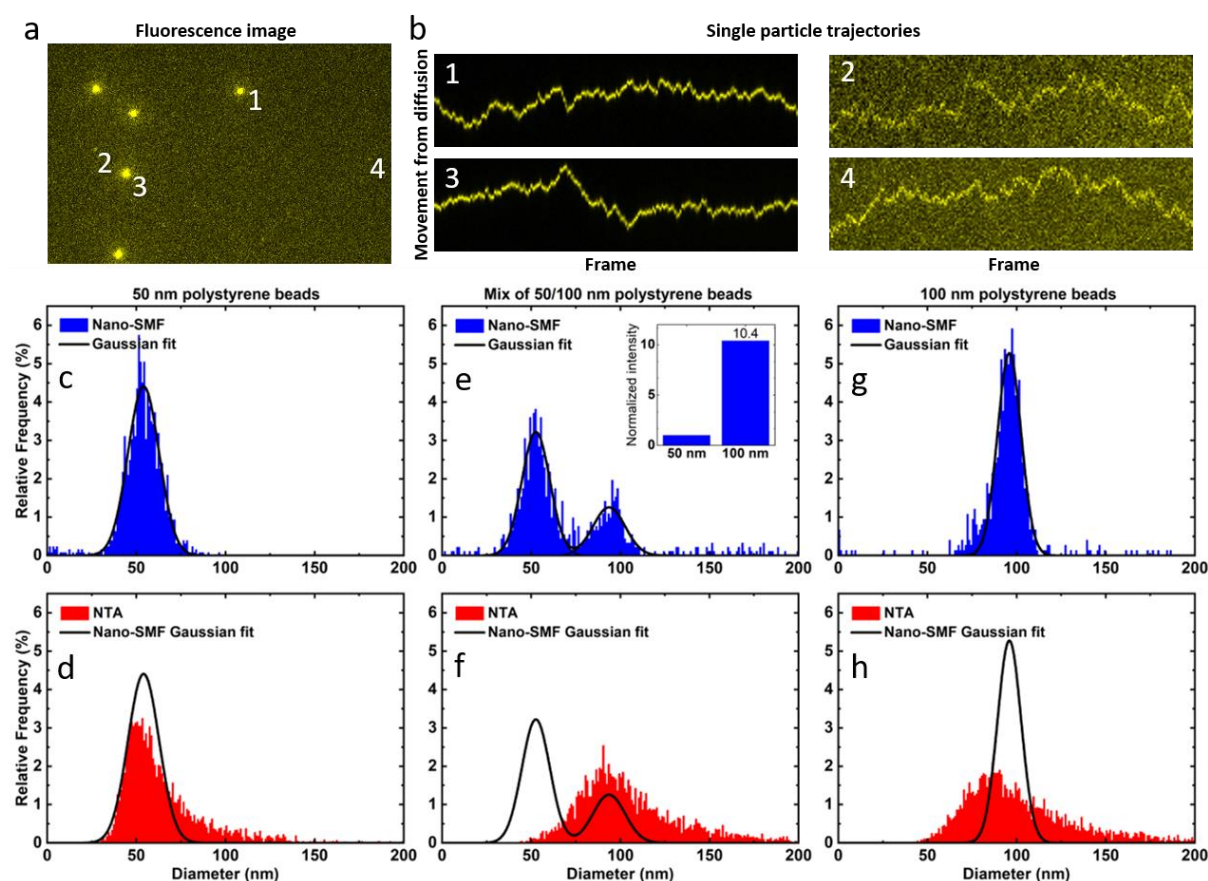
Figure 6.2. Comparison of size distributions for 50 and 100 nm polystyrene beads obtained using Nano-SMF (blue) and NTA (red). a) Snapshot of mixed 50 and 100 nm polystyrene beads using Nano-SMF. b) Trajectories displaying Brownian motion from numbered particles in (a). c-d) Size distribution of 50 nm polystyrene beads obtained with Nano-SMF (c) and NTA (d). e-f) Size distribution of mixed 50 and 100 nm polystyrene beads obtained with Nano-SMF (e) (inset displays the difference in fluorescence intensity between the 50 and 100 nm particles) and NTA (f). g-h) Size distribution of 100 nm polystyrene beads obtained with Nano-SMF (g) and NTA (h). Size distributions obtained with Nano-SMF (c, e and g) are fitted with Gaussian distributions and displayed for comparison with NTA (d, f and h).

By using a multi bandpass filter and sequentially switching light source, Nano-SMF can determine the fluorescence intensity for multiple fluorescent labels. Through colocalization between exosomes with the different fluorescent labels, we observed distinct sub-populations, which differed in mean size depending on which of the exosome biomarker tetraspanin proteins CD63 and CD81 that resided on them. Additionally, the different biomarkers displayed variation in their size-intensity scaling, revealing a difference in how tetraspanins may be distributed into exosomes during biogenesis. These findings display that Nano-SMF is a versatile platform where subpopulations within polydisperse samples such as exosomes can be investigated, and multiple independent properties, connected to size and intensity, can be evaluated simultaneously from a single measurement.

6.1.3 Paper 3

To provide single particle catalysis measurement on particles with defined surface facets, the method for parallelized nanofluidic fluorescence microscopy, presented in **Paper 1**, was extended upon. The main features of the previous design were retained to preserve the benefits provided by keeping the fluorescent molecules in the focal plane of the microscope and ensuring identical reaction conditions. Trapping of single colloidal nanoparticles larger than 30 nm in diameter was achieved by addition of vertical constrictions in the nanochannel centers, leaving a 30 nm high slit. The attachment to the nanochannel walls was then enhanced by addition of salt (NaCl, 5M) to decrease the electrostatic screening between the particles and the walls. The particle trapping was monitored with dark field microscopy to collect scattering intensity steps, from which the number of trapped particles in each channel were determined. Additionally, the particle trapping was confirmed with SEM via entrapment in a polysilsesquioxane (PSQ) bonded chip from which the lids could be detached. By trapping 32 colloidal Au nanospheres of 100 nm in diameter, the transition from a surfaced poisoned regime into a mass transport limited regime of catalysis was monitored with single particle precision. A spread in single-particle-specific activity was observed and linked to the widely varying surface faceting of the colloidal spheres. Day to day variation in the concentration at maximum ToF was observed, but the respective activity of the individual particles was retained between all measurements. This observation highlighted the need for simultaneous measurment of single nanoparticles to correctly compare their catalytic activity.

By trapping single Au colloidal nanoparticles sequentially, several nanoparticles with varying shape and surface facets (spheres, cubes and octahedra), were trapped side by side in an array of 100 nanochannels (Figure 6.3). Catalytic reduction on the faceted Au nanoparticles displayed a difference in the concentration at maximum turnover frequency (ToF), at which the catalytic activity transitioned from a surface poisoned to a mass transport limited regime of catalysis. The concentration at maximum ToF was hypothesized to depend on the adsorption energy of fluorescein, which was shown to decrease for surfaces with higher curvature, such as steps, corners and edges, using first-principles calculations. We therefore suggested that transition at higher fluorescein concentrations could be attributed to the high abundance of edges and corner sites on cubes and octahedra, as compared to spherical nanoparticles (inset in Figure 6.3a). The differences in concentration at maximum ToF observed between the trapped particles, demonstrated that parallelized nanofluidic fluorescence microscopy enables assessment of structure sensitivity between several single nanoparticles measured at identical reaction conditions. The utilization of dark field microscopy in combination with fluorescence microscopy to initially monitor particle trapping and subsequently catalytic activity, showcase the usefulness in combining multiple techniques for readout of different single particle properties.
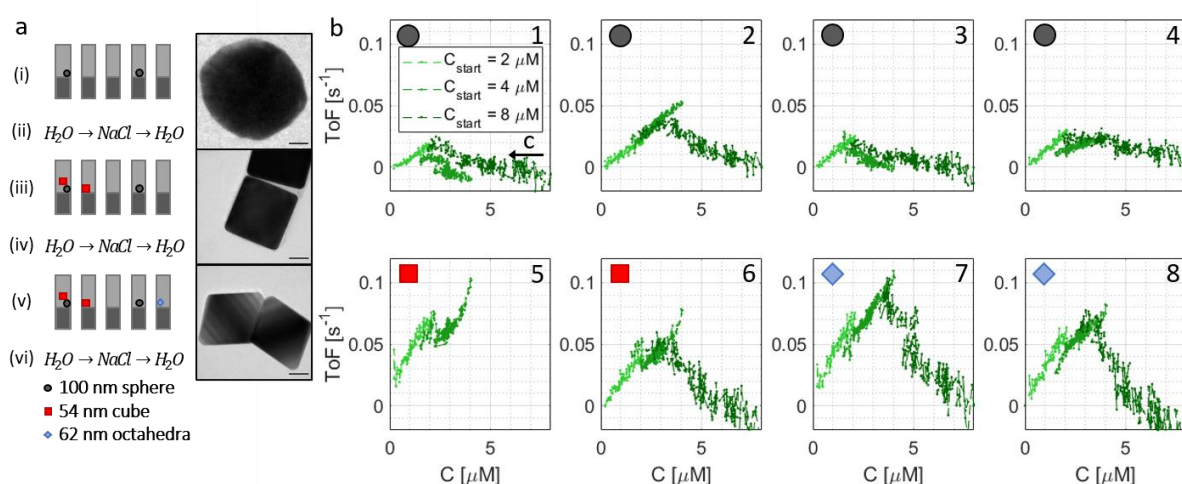

Figure 6.3. Fluorescein reduction with sodium borohydride on single Au spheres, cubes and octahedra. a) Schematic of the process flow during the consecutive trapping of colloidal particles with different shape: (i) trapping of 100 nm faceted Au spheres; (ii) flushing with NaCl solution to induce strong particle attachment; (iii) trapping of 54 nm Au cubes; (iv) flushing with NaCl solution to induce stronger particle attachment;(v) trapping of 62 nm Au octahedra; (vi) flushing with NaCl solution to induce strong particle attachment. b) ToF for trapped single faceted Au spheres, cubes and octahedra, measured simultaneously in the same chip upon three subsequent fluorescein concentration sweeps starting at Cstart = 2 μM, 4 μM, and 8 μM, respectively.

6.2 Additional contributions

The main part of my PhD work has been dedicated to establishing new methods to measure nanoparticle properties that are hard to acquire with existing techniques. As the methods have been established, the aim has been to display their usefulness by measuring important nanoparticle properties. In these endeavors, I have investigated several different approaches before pursuing the ones that showed the most promise. I will here present some of the trials where there is not yet enough data to draw clear conclusions, but which contain elements that are worthwhile bringing forth for discussion.

6.2.1 Catalysis on single nanoparticles of different metals

In the nanochannel device presented in **Paper 3** it is possible to trap nanoparticles of different metals, such as Ag and Pt, in addition to Au nanoparticles. In principle, any particles with sufficient negative charge, such that they do not initially stick to the channel walls, can be trapped in this device. Spherical citrate stabilized Ag and Au nanoparticles (80 nm in diameter), and Pt nanoparticles (70 nm in diameter), were trapped alongside each other through sequential trapping. After entrapment, rigorous cleaning of the nanoparticles (and the nano-/microchannels) was needed before catalytic reduction of fluorescein was observed. For Au nanoparticles, I established (in **Paper 1**) that the cleaning can be done by flushing for 20 minutes with a solution of Hydrogen peroxide (30 wt. %), ammonia (30 wt. %), and water in a ratio of 1:1:5. Therefore, the same procedure was applied for Ag and Pt, with some uncertainty whether it would be suited for cleaning those metals, since the solution etches the Au surface slightly and should etch other metals more efficiently.
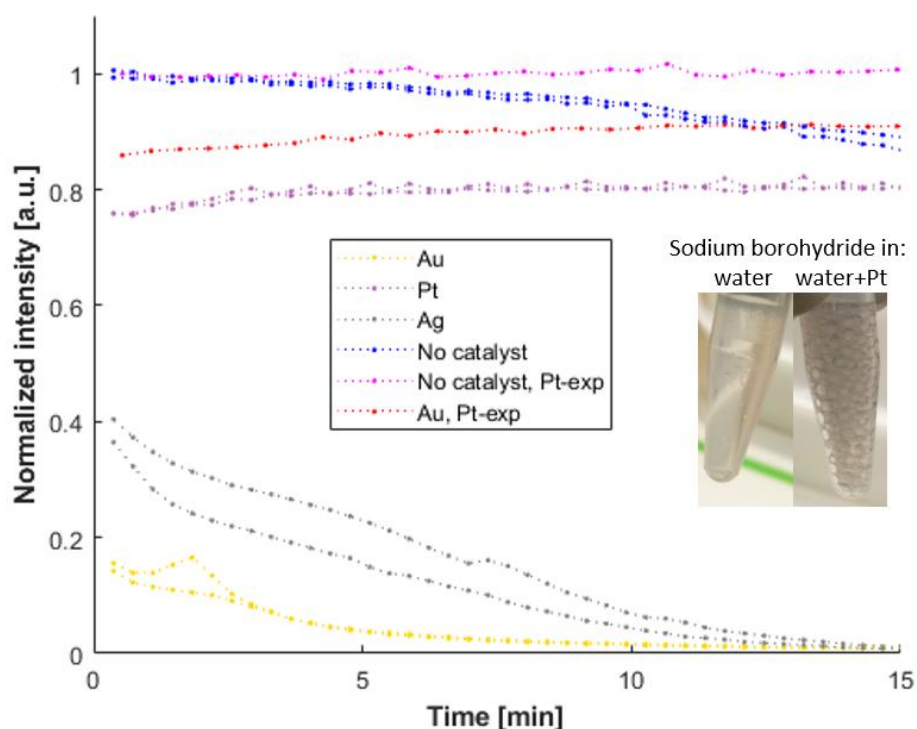
Figure 6.4. Batch reduction of fluorescein by Au, Ag and Pt. Substantial activity is observed for both Au and Ag nanoparticles, but not for Pt. Inset shows the gas development for sodium borohydride exposed to Pt nanoparticles as compared to sodium borohydride in water. No catalytic activity is observed when using the Pt-exposed sodium borohydride together with Au nanoparticles or without catalyst.

To evaluate if other metals than Au would be active in the reduction of fluorescein by borohydride, they were initially tested in a batch setting (Figure 6.4). The batch experiments were done by mixing the reaction reagents (10 μM sodium fluorescein and 50mM sodium borohydride) with and without the catalysts (colloidal Au, Ag or Pt suspension) in several wells in a microwell plate and measuring the fluorescence with a microplate reader. In the batch experiments, Ag particles displayed a slightly slower reduction rate than Au and Pt displayed no activity at all. We speculate that the inactivity in the mixture with Pt derives from Pt consuming the borohydride and producing H_2 gas[165], instead of reducing the fluorescein. This hypothesis was strengthened by showing that a borohydride solution mixed with Pt nanoparticles displayed excessive gas generation. Furthermore, the Pt-exposed sodium borohydride solution was thereafter unable to be used for reduction of fluorescein (Figure 6.4).

The issue of borohydride consumption formed an interesting prospect, since it could possibly be solved by the directed flow in the nanochannels, where fresh reactants are supplied continuously. However, when subjecting the Pt nanoparticles to the cleaning solution in the nanochannels, H_2 gas was generated[166, 167]. The gas dissolved after

flushing with water, but the gas development removed most of the Pt nanoparticles. When fluorescein and sodium borohydride were later introduced, the channels where Pt nanoparticles were still visible in dark field microscopy showed catalytic activity (Figure 6.5a). However, since nearly all Pt particles were removed by the gas, only a few particles were left for evaluation.

An intriguing feature observed during the gas formation was that for channels containing both Au and Pt the generated gas pushed out the Au nanoparticles (Figure 6.6). This interaction could possibly be extended upon and developed into a system for purposefully propelling nanoparticles in a fluidic system using local gas generation inside the nanofluidic system.
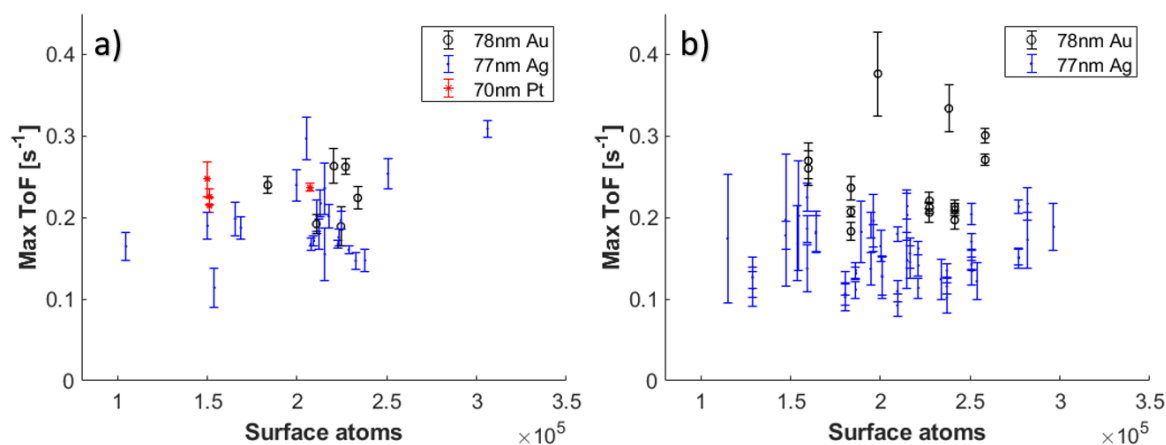
Figure 6.5. Maximum turnover frequency for single Au, Ag and Pt nanoparticles. a) Nearly all particles were mass transport limited throughout this experiment. The Pt particles that remained after cleaning showed substantial catalytic activity. b) Comparison in activity between Au and Ag nanoparticles. It is, however, unclear in which state of oxidation the Ag nanoparticles are in (Ag, Ag-oxide and/or fragmented).
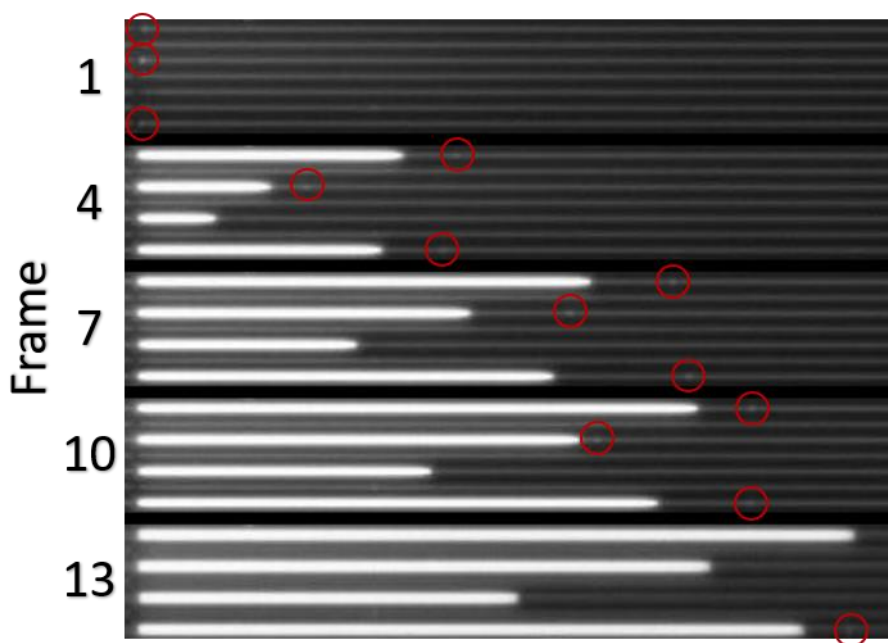
Figure 6.6. Au nanoparticles being propelled by gas generation from Pt nanoparticles. In three of the nanochannels (nr 1, 3 and 7 from above) an Au nanoparticle, highlighted by red circles, can be observed moving to the right in front of the increasing gas bubble produced during the nanoparticle cleaning.

Ag nanoparticles showed catalytic activity for fluorescein reduction in batch to a similar degree as Au nanoparticles (Figure 6.4). However, when the Ag nanoparticles were trapped in the nanofluidic chip and subjected to the cleaning solution, they displayed an apparent decrease in scattering intensity. This decrease was interpreted as oxidation (or partial oxidation) of the Ag particles. For the reduction of fluorescein, they displayed a catalytic activity slightly lower than that of Au nanoparticles (Figure 6.5b), comparable to the batch experiment. To verify the oxidation of the Ag particles, Ag and Au nanoparticles were trapped and cleaned in a PSQ bonded chip for evaluation with SEM. Unfortunately, nearly all particles were removed as the lids were removed for several PSQ bonded chips, and the few nanoparticles that stayed in place and could be verified with SEM, were all Au. This indicated that the Ag nanoparticles likely were completely dissolved by the cleaning solution. In another trial, an Ag surface exposed to the cleaning solution was completely dissolved (Figure 6.7). Both trials therefore suggest that the Ag is dissolved completely by the cleaning solution. This leaves us with the conundrum why the channels that initially contained Ag particles are still displaying a distinct activity for fluorescein reduction (Figure 6.5b). A possible explanation is that the Ag is partially dissolved and dispersed along the nanochannel, giving the channel an activity from multiple Ag/Ag-oxide fragments etched from the original Ag particle.
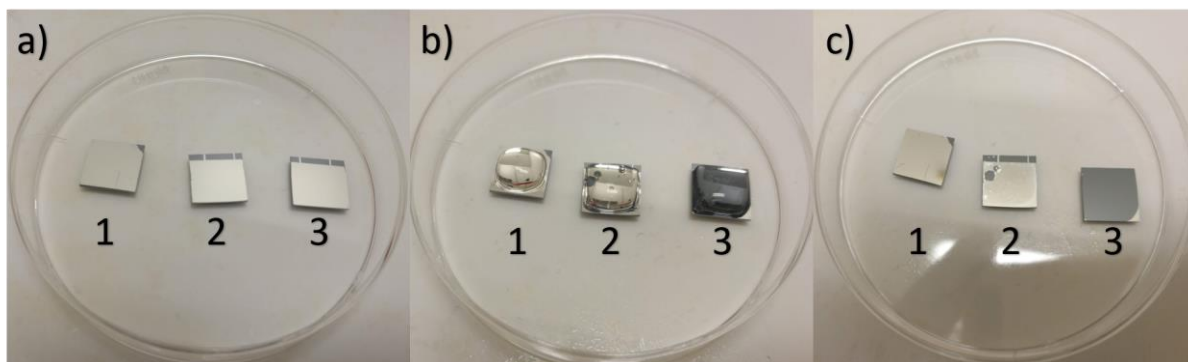
Figure 6.7. Cleaning of 50 nm thick Ag surface with (1) water, (2) cleaning solution and water 1:9, and (3) cleaning solution. a) before cleaning. b) during cleaning. c) after cleaning. The Ag in (1) is unaffected, in (2) is slightly etched and partially oxidized, and in (3) is completely dissolved where the cleaning solution has been.

6.2.2   Catalysis at varying flow speed

An advantage with the parallelized nanofluidic fluorescence microscopy is that the flow speed can be varied, to alter the mass transport of reactants to the nanoparticles. This is exemplified in Figure 6.8, where ToF for six different particles at flow speeds of 68, 136 and 272 µm/s (flow pressures of 500, 1000 and 2000 mbar) is shown. Measurements were done in the order 272, 136 and 68 µm/s, and a final measurement at 272 µm/s was made to confirm that the reaction conditions had not change between experiments. At a lower flow speed, the number of molecules that reach the catalyst per second is decreased. Therefore, the slope in ToF versus fluorescein concentration is lower for lower flow speeds in the mass transport limited regime. Each particle displays a plateau in the ToF, which is reached at higher flow speed, but not at lower flow speed due to the low supply of fluorescein molecules. The transition from the surface poisoned regime (fluorescein concentration > 23 µM) into the reaction limited regime (fluorescein concentration ~15 µM at a flow speed of 272 µm/s) or directly into the mass transport limited regime (linearly increasing ToF at lower fluorescein concentrations) happens in a different span of concentrations, which depends on the flow speed. At a flow speed of 272 µm/s, the transition happens gradually, across a span of fluorescein concentrations between ~23 and 30 µM, while at a flow speed of 68 µm/s, the fluorescein concentration remains constant at around 23 µM during the transition. This difference is an artefact, inherent to how the incoming fluorescein concentration decreases over time. The decrease in concentration is a consequence of the partial reduction of the fluorescein at unspecific active sites along the large surface

area present in the microchannels, prior to entering the nanochannels. This reduction happens at a lower rate than at the nanoparticles, and results in an "automatic scan" of the incoming fluorescein concentrations during each measurement (Supplementary information of **Paper 1**). Furthermore, the decrease of the incoming fluorescein concentration accelerates with time, due to the higher activity at lower fluorescein concentrations. Therefore, depending on when the transition between different regimes occurs, the transition will span a varying range of fluorescein concentrations. This becomes apparent when considering the concentration that is reduced at any given timepoint (Figure 6.9). The transition then happens in the same time frame seemingly independent of the flow speed, but instead depending on the single particle. The similarity in reduced fluorescein concentration during the transition could indicate that the activity during transition is mainly governed by diffusion to the uninhibited catalyst sites. The difference between particles does in turn suggest a difference in reaction rate resulting in different transition rate from the surface poisoned to the mass transport limited regime.
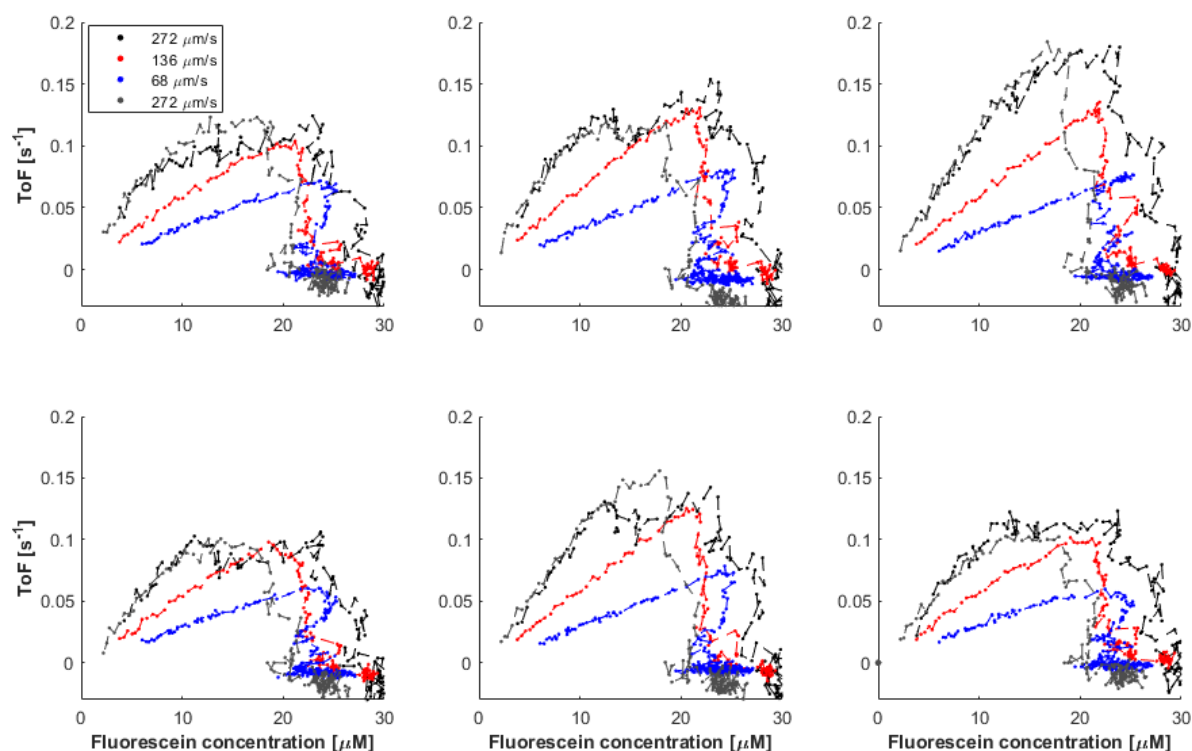

Figure 6.8. ToF derived at different flow speeds (272, 136 and 68 μm/s, and again at 272 μm/s) for six single spherical Au nanoparticles.

Additional experiments are needed to verify the findings at varying flow speeds discussed above. However, reproducing this kind of reactivity profiles at varying flow speed is time consuming, as the concentration where the transition occurs varies from day to day, as discussed in **Paper 3**. Additionally, the particles featured in these experiments (Figure 6.8 and Figure 6.9) were not monitored during trapping and are therefore not guaranteed to be single particles, although the similarity between the ToF profiles indicates that they are.
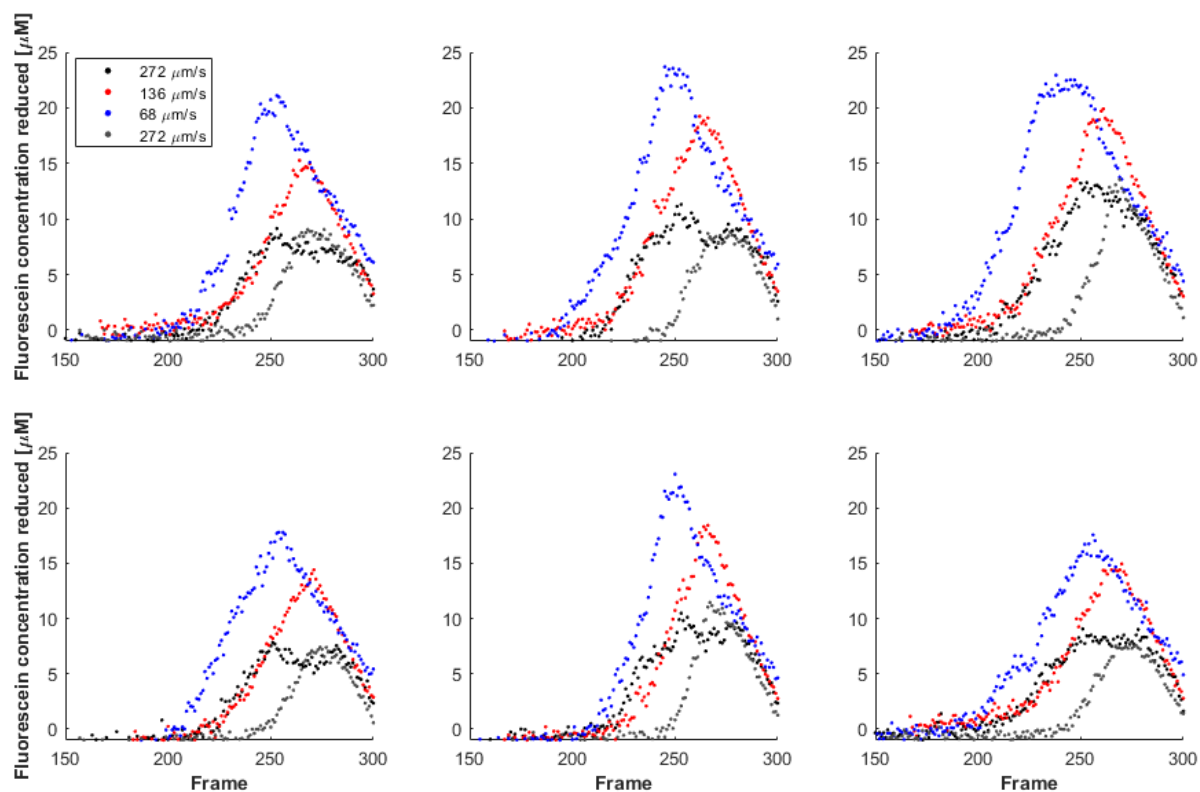
Figure 6.9. Fluorescein concentration reduced by the nanoparticle at each given frame during measurements at different flow speed (272, 136 and 68 μm/s, and again at 272 μm/s), for the same six nanoparticles as in Figure 6.8.

Another possibility the control of flow speed provides, is to vary the flow during the experiment. Figure 6.10 showcases the ToF for ten single Au spheres (100 nm in diameter), measured during an experiment where the flow speed was varied back and forth between 272 μm/s and 68 μm/s. Note how the transition into the mass transport limited regime (black and blue dashed lines) occurs differently, both between particles and between flow speeds. At a flow speed of 68 μm/s, most particles are in the mass transport limited regime already around frame 50, while no particle completely reaches the mass transport limited regime until frame 170 at a flow speed of 272 μm/s.

Switching the speed back and forth also reveals how a higher mass transport can result in a lower apparent activity, as observed for most particles the first time the flow speed is switched from 68 μm/s to 272 μm/s. This indicates a strong relation between the surface poisoning at high fluorescein concentration and the supply of reactants to maintain it. The increase in ToF when switching back to 68 μm/s in turn demonstrates a reversibility between the different reactivity regimes and that the transition can be regulated by the flow speed.
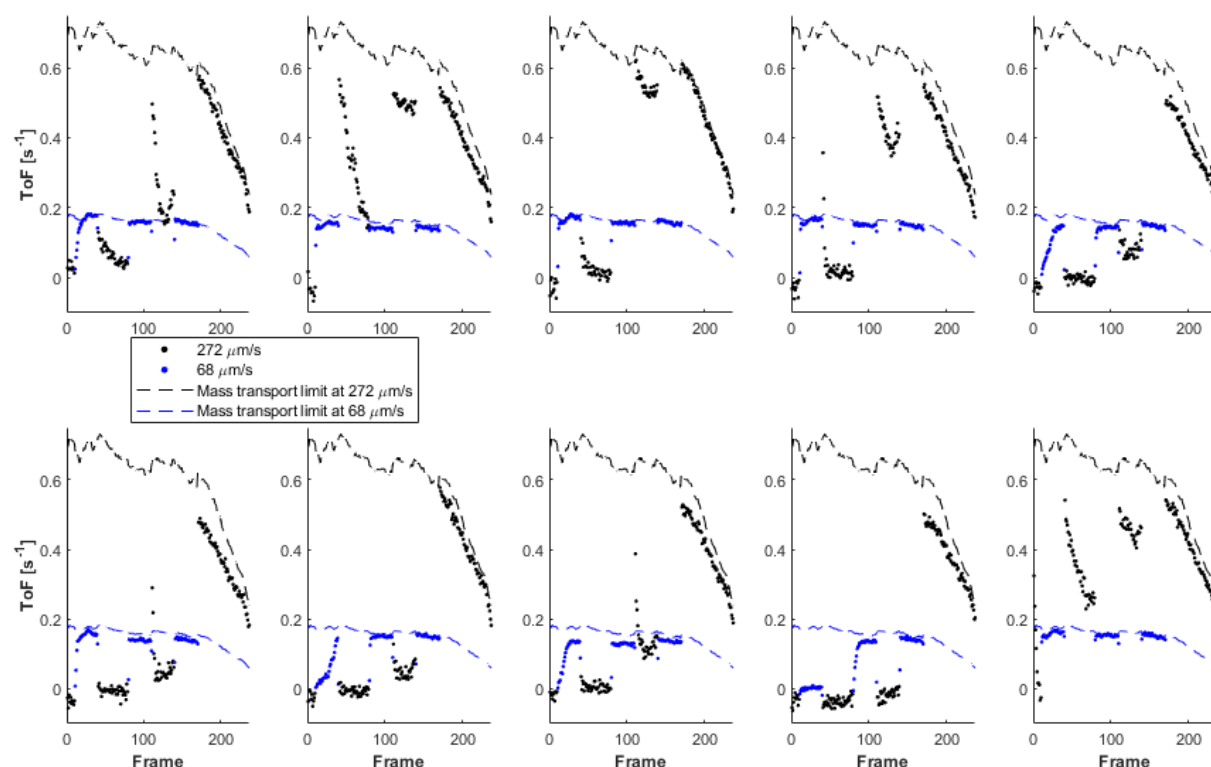

Figure 6.10. ToF during each time frame of fluorescein reduction when the flow speed was switched back and forth between 2000 mbar (black dots) and 500 mbar (blue dots). Note how the transition into the mass transport limited regime (black and blue dashed lines) varies between particles and flow speeds.

6.2.3 Specialized script for 1D particle tracking

Particles tracked with Nano-SMF are restricted to movement in one direction by being confined in an array of nanochannels. It is therefore possible to simplify the particle tracking and only consider the movement occurring specifically along the nanochannels and in just one dimension (1D). To explore this option, a MATLAB script for 1D tracking for a simplified and quicker analysis is being developed. The script restructures the recorded movies into multiple kymographs (Figure 6.11a), one for each nanochannel, which has the extension of the nanochannel on one axis and the time domain (one frame per line) on the other axis. The particles flowing through the nanochannel will appear as diagonal lines in the kymograph and can then be detected by convolution with a diagonal segmentation matrix (Figure 6.11b), constructed by a diagonal gap with the same inclination as the particle traces. Convolving the kymograph with the segmentation matrix results in an intensity profile across all movie frames which can be evaluated to detect each particle trace (Figure 6.11c).
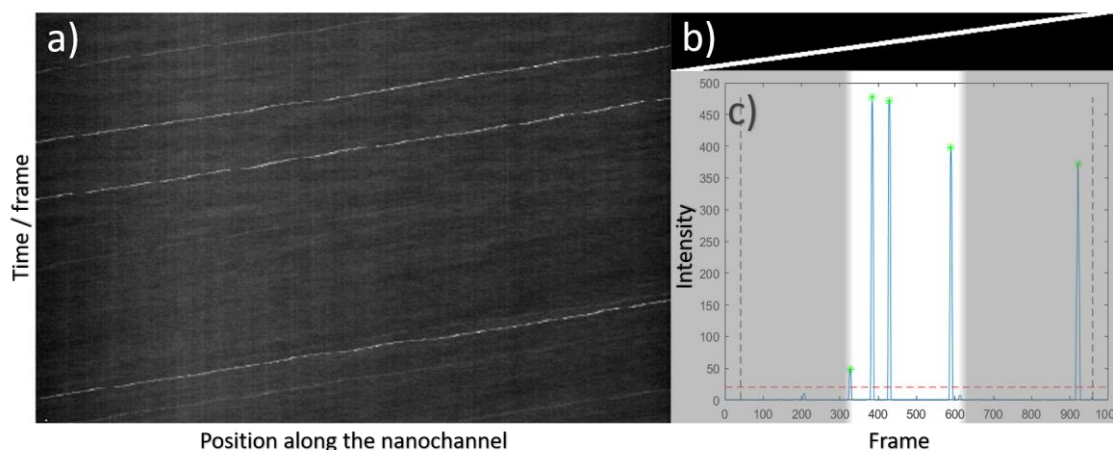

Figure 6.11. Summary of how particles can be tracked by collapsing single nanochannels into kymographs. a) Part of a kymograph from a single nanochannel. The white lines are traces of fluorescent particles passing through the channel. b) Segmentation matrix used to convolve with the kymographs to find particle traces. c) Evaluation of the convolved kymograph and segmentation matrix. The white area represents the part of the kymograph visible in (a). The dotted red line is a cutoff for the signal needed for a trace to be evaluated and each evaluated trace is marked with a green star.

After detection of the particle traces, the kymograph can be divided into single trajectory sections in which the maximum intensity for each time frame can be evaluated as the particle position. To achieve sub-pixel resolution, the particle position is then iterated with a Gaussian approximation fit[168]. Additionally, the Gaussian fit provides detailed intensity values. The particle positions can then be determined using the same equations as in Nano-SMF (**Paper 2**) to get size distributions from all tracked particles (Figure 6.12). While the size distributions provided from the two scripts were very comparable, the script operating only in 1D runs about 20 times faster. However, for samples with a wide variation in intensities (Figure 6.12c), the current image segmentation in the 1D script could not detect the majority of the dimmer particle traces. Since the detection of complex samples, containing variation in size and intensity, is one of the main strengths of Nano-SMF, the image segmentation of samples with spread in intensity needs improvement before more rigorous applications using the 1D tracking script.
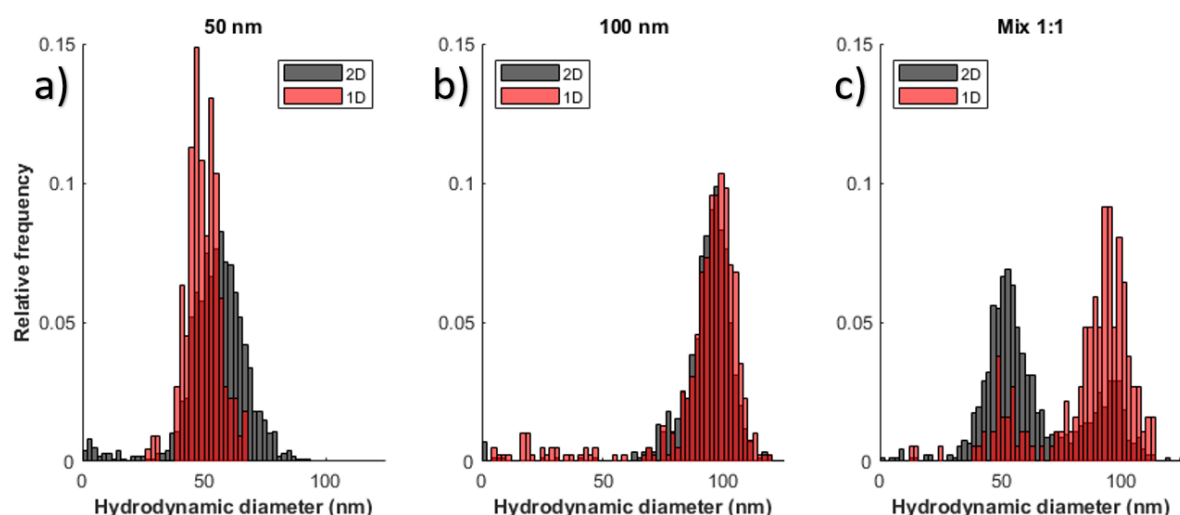

Figure 6.12. Examples of size distributions provided from the script tracking only in 1 dimension (red) versus the one tracking in 2 dimensions (gray). a) Size distributions from 50 nm polystyrene beads. b) Size distributions from 100 nm polystyrene beads. c) Size distribution from mixed sample of both 50 and 100 nm polystyrene beads.

7 Outlook

In this thesis, I have presented two methods for characterization of single nanoparticle properties, such as catalytic activity, fluorescence intensity and size. The experiments with these methods have up until now been mainly made in a proof-of-concept manner, to establish the techniques and give an idea of their capabilities. As displayed in the section *6.2 additional contributions*, there are several interesting aspects in these methods to explore and develop, where more experiments are needed. For example, the idea of observing the catalytic activity of different metals can be developed further by assessing alternative solutions for cleaning the particle surfaces. Additionally, it can be extended to alloy particles and the exploration of the impact of the ratio between different metals in alloys. Alternatively, the impact of different ligands on the particle surface, which can either hinder or benefit the catalytic activity[76, 169], can be explored. With the capability of trapping particles with different ligands, as well as a flow system to potentially exchange the ligands on trapped particles, the activity of one and the same nanoparticle but with different ligands can be investigated. With protocols to clean the particle surface, the difference with or without ligand capping can be studied and provide new insights in the role of ligands in nanoparticle catalysis.

Another direction in which parallelized nanofluidic fluorescence microscopy can be developed is in extended control of reaction parameters, such as flow, temperature, and reactant concentrations. With additional parameters to vary, the different regimes of catalysis can be mapped in more detail to give a more complete understanding of the reaction mechanisms. For example, temperature variation can provide information on activation energy of the reaction. Higher temperatures can also assist in the exploration of additional reactions, by increase of the reaction rate. With control of temperature to alter reaction rate, and flow speed to alter mass transport in real time, as well as increased control over reactant concentrations, the boundaries between the different catalysis regimes can be intricately maneuvered to answer complex questions regarding mass transport and surface poisoning at the single nanoparticle level.

While parallelized nanofluidic fluorescence microscopy is, in its current version, restricted to a read-out signal from fluorescence, there are still a lot of relevant questions that the method can assist in answering. Variation in flow speed, interaction between reactants and nanochannel walls can be explored further and the similarity between the nanochannel and a catalyst pore can bridge the understanding of mass transport into porous scaffolds[133]. Placement of several particles along one and the same nanochannel can in turn simulate particles early and late in a catalyst bed and answer questions about how a reaction on one particle affects the reaction downstream[170]. The restriction to fluorescence can also be circumvented by designs where the fluorescent species simply competes with a non-fluorescent reaction of interest[171]. Ideally, the method is combined with other methods that can complement the readout signal, such as plasmonic nanospectroscopy[134] or surface enhanced Raman spectroscopy[130] to get information of the molecular species on the surface of the catalyst, or in situ TEM[137] to monitor the surface structure during the reaction.

The prospect of nanocatalysis is generally to develop efficient and cost effective catalysts for a more sustainable material use, chemical production or energy consumption[172]. Since smaller nanoparticles (<10 nm) are more efficient, with respect to surface area per volume (i.e. material use), and also generally display increased activity, being able to measure single nanoparticle catalysis at these sizes is of huge interest. However, this prospect comes with substantial challenges as the reaction rate needed for parallelized nanofluidic fluorescence microscopy is substantial. Additionally, the nanoparticle trapping depends on scattering, which decreases dramatically with particle size. Methodologies such as particle antennas or fluorescently marked particles to increase the signal, or porous shells to increase residence time can alleviate these issues, but at the cost of a more complicated measurement system.

Nano-SMF provides a versatile method for size determination of nanoparticles of size 20-200 nm in diameter. The method is very useful to study exosomes, as no extensive sample preparation is needed before characterization and the technique provides both fluorescence intensity in multiple colors as well as detailed size distributions. With its capability to characterize and count exosomes in nanoliter volumes of cell media, the method can provide new applications within diagnostics and exosome research. Nano-SMF can also analyze other soft biological nanoparticles, and possibly provide analysis of size and compositional variation in relating fields, such as virology and drug delivery. Since the tracking only needs to be done in one dimension, the speed of analysis can be vastly improved, and if real time analysis can be achieved, the technique can possibly facilitate particle sorting based on both particle composition and size.

Parallelized nanofluidic fluorescence microscopy and Nano-SMF can still be improved and developed further, but they are already highly functional methods to extract single nanoparticle properties, which are hard to obtain by other means. Together, they demonstrate how nanofluidics can provide versatile platforms for studying and characterizing various nanoparticle properties and can hopefully inspire others to utilize similar methodologies.

8 Acknowledgements

9 References

1. Khan, I., Saeed, K. & Khan, I. Nanoparticles: Properties, applications and toxicities. *Arabian Journal of Chemistry* **12**, 908-931 (2019).
2. Lewis, L.N. Chemical catalysis by colloids and clusters. *Chemical Reviews* **93**, 2693-2730 (1993).
3. Yao, K. et al. Plasmonic Metal Nanoparticles with Core–Bishell Structure for High-Performance Organic and Perovskite Solar Cells. *ACS Nano* **13**, 5397-5409 (2019).
4. Odularu, A.T. Metal Nanoparticles: Thermal Decomposition, Biomedicinal Applications to Cancer Treatment, and Future Perspectives. *Bioinorganic Chemistry and Applications* **2018**, 9354708 (2018).
5. Sztandera, K., Gorzkiewicz, M. & Klajnert-Maculewicz, B. Gold Nanoparticles in Cancer Treatment. *Molecular Pharmaceutics* **16**, 1-23 (2019).
6. Ohe, T., Miyaura, N. & Suzuki, A. Palladium-catalyzed cross-coupling reaction of organoboron compounds with organic triflates. *The Journal of Organic Chemistry* **58**, 2201-2208 (1993).

7.   Astefanei, A., Núñez, O. & Galceran, M.T. Characterisation and determination of fullerenes: A critical review. *Analytica Chimica Acta* **882**, 1-21 (2015).

8.   Mashaghi, S., Jadidi, T., Koenderink, G. & Mashaghi, A. Lipid Nanotechnology. *Int J Mol Sci* **14** (2013).

9.   Rao, J.P. & Geckeler, K.E. Polymer nanoparticles: Preparation techniques and size-control parameters. *Progress in Polymer Science* **36**, 887-913 (2011).

10.   Sun, B. et al. Applications of stem cell-derived exosomes in tissue engineering and neurological diseases. *Reviews in the Neurosciences* **29**, 531-546 (2018).

11.   Gurunathan, S., Kang, M.-H., Jeyaraj, M., Qasim, M. & Kim, J.-H. Review of the Isolation, Characterization, Biological Function, and Multifarious Therapeutic Approaches of Exosomes. *Cells* **8** (2019).

12.   Silvera Batista, C.A., Larson, R.G. & Kotov, N.A. Nonadditivity of nanoparticle interactions. *Science* **350**, 1242477 (2015).

13.   Alekseeva, S. et al. Grain boundary mediated hydriding phase transformations in individual polycrystalline metal nanoparticles. *Nature Communications* **8**, 1084 (2017).

14.   Syrenova, S. et al. Hydride formation thermodynamics and hysteresis in individual Pd nanocrystals with different size and shape. *Nature Materials* **14**, 1236-1244 (2015).

15.   Nilsson Pingel, T., Jørgensen, M., Yankovich, A.B., Grönbeck, H. & Olsson, E. Influence of atomic site-specific strain on catalytic activity of supported nanoparticles. *Nature Communications* **9**, 2722 (2018).

16.   Rabanel, J.-M. et al. Nanoparticle heterogeneity: an emerging structural parameter influencing particle fate in biological media? *Nanoscale* **11**, 383-406 (2019).

17.   Adjei, I.M., Peetla, C. & Labhasetwar, V. Heterogeneity in nanoparticles influences biodistribution and targeting. *Nanomedicine (Lond)* **9**, 267-278 (2014).

18.   Buurmans, I.L.C. & Weckhuysen, B.M. Heterogeneities of individual catalyst particles in space and time as monitored by spectroscopy. *Nature Chemistry* **4**, 873-886 (2012).

19.   Carter, C.B. & Williams, D.B. Transmission Electron Microscopy. [electronic resource] : Diffraction, Imaging, and Spectrometry, Edn. 1st ed. 2016. (Springer International Publishing, 2016).

20.   Chen, Y. Nanofabrication by electron beam lithography and its applications: A review. *Microelectronic Engineering* **135**, 57-72 (2015).

21.   Pease, R.F.W. Electron beam lithography. *Contemporary Physics* **22**, 265-290 (1981).

22. De Cremer, G., Sels, B.F., De Vos, D.E., Hofkens, J. & Roeffaers, M.B.J. Fluorescence micro(spectro)scopy as a tool to study catalytic materials in action. *Chemical Society Reviews* **39**, 4703-4717 (2010).

23. Tachikawa, T. & Majima, T. Single-Molecule, Single-Particle Approaches for Exploring the Structure and Kinetics of Nanocatalysts. *Langmuir* **28**, 8933-8943 (2012).

24. Huang, T., Nallathamby, P.D., Gillet, D. & Xu, X.-H.N. Design and Synthesis of Single-Nanoparticle Optical Biosensors for Imaging and Characterization of Single Receptor Molecules on Single Living Cells. *Analytical Chemistry* **79**, 7708-7718 (2007).

25. Yurt, A., Daaboul, G.G., Connor, J.H., Goldberg, B.B. & Selim Ünlü, M. Single nanoparticle detectors for biological applications. *Nanoscale* **4**, 715-726 (2012).

26. van der Pol, E., Coumans, F.A.W., Sturk, A., Nieuwland, R. & van Leeuwen, T.G. Refractive Index Determination of Nanoparticles in Suspension Using Nanoparticle Tracking Analysis. *Nano Letters* **14**, 6195-6201 (2014).

27. Dragovic, R.A. et al. Sizing and phenotyping of cellular vesicles using Nanoparticle Tracking Analysis. *Nanomedicine: Nanotechnology, Biology and Medicine* **7**, 780-788 (2011).

28. Feynman, R.P. There's plenty of room at the bottom. *Resonance* **16**, 890 (2011).

29. Prakash, S. & Yeom, J. Nanofluidics and Microfluidics: Systems and Applications. (2014).

30. Nanofluidics is on the rise. *Nature Materials* **19**, 253-253 (2020).

31. Xu, Y. Nanofluidics: A New Arena for Materials Science. *Advanced Materials* **30**, 1702419 (2018).

32. Mawatari, K., Kazoe, Y., Shimizu, H., Pihosh, Y. & Kitamori, T. Extended-Nanofluidics: Fundamental Technologies, Unique Liquid Properties, and Application in Chemical and Bio Analysis Methods and Devices. *Analytical Chemistry* **86**, 4068-4077 (2014).

33. Zhong, J. et al. Exploring Anomalous Fluid Behavior at the Nanoscale: Direct Visualization and Quantification via Nanofluidic Devices. *Accounts of Chemical Research* **53**, 347-357 (2020).

34. Eijkel, J.C.T. & Berg, A.v.d. Nanofluidics: what is it and what can we expect from it? *Microfluidics and Nanofluidics* **1**, 249-267 (2005).

35. Albinsson, D. (Chalmers University of Technology, 2020).

36. Hibara, A. et al. Nanochannels on a Fused-Silica Microchip and Liquid Properties Investigation by Time-Resolved Fluorescence Measurements. *Analytical Chemistry* **74**, 6170-6176 (2002).

37.	Tas, N., Haneveld, J., Jansen, H.V., Elwenspoek, M. & Van den Berg, A. Capillary filling speed of water in nanochannels. *Applied Physics Letters* **85**, 3274-3276 (2004).

38.	Xu, Y. & Xu, B. An Integrated Glass Nanofluidic Device Enabling In-situ Electrokinetic Probing of Water Confined in a Single Nanochannel under Pressure-Driven Flow Conditions. *Small* **11**, 6165-6171 (2015).

39.	Zhang, M. et al. Light and pH Cooperative Nanofluidic Diode Using a Spiropyran-Functionalized Single Nanochannel. *Advanced Materials* **24**, 2424-2428 (2012).

40.	Gamble, T. et al. Rectification of Ion Current in Nanopores Depends on the Type of Monovalent Cations: Experiments and Modeling. *The Journal of Physical Chemistry C* **118**, 9809-9819 (2014).

41.	Kim, S.J., Wang, Y.-C., Lee, J.H., Jang, H. & Han, J. Concentration polarization and nonlinear electrokinetic flow near a nanofluidic channel. *Phys Rev Lett* **99**, 044501-044501 (2007).

42.	Louër, A.-C. et al. Pressure-Assisted Selective Preconcentration in a Straight Nanochannel. *Analytical Chemistry* **85**, 7948-7956 (2013).

43.	Bocquet, L. & Tabeling, P. Physics and technological aspects of nanofluidics. *Lab on a Chip* **14**, 3143-3158 (2014).

44.	Haywood, D.G., Saha-Shah, A., Baker, L.A. & Jacobson, S.C. Fundamental Studies of Nanofluidics: Nanopores, Nanochannels, and Nanopipets. *Analytical Chemistry* **87**, 172-187 (2015).

45.	Sparreboom, W., van den Berg, A. & Eijkel, J.C.T. Principles and applications of nanofluidic transport. *Nature Nanotechnology* **4**, 713-720 (2009).

46.	Regtmeier, J., Käsewieter, J., Everwand, M. & Anselmetti, D. Continuous-flow separation of nanoparticles by electrostatic sieving at a micro-nanofluidic interface. *Journal of Separation Science* **34**, 1180-1183 (2011).

47.	Viefhues, M., Regtmeier, J. & Anselmetti, D. Fast and continuous-flow separation of DNA-complexes and topological DNA variants in microfluidic chip format. *The Analyst* **138**, 186-196 (2013).

48.	Friedrich, R. et al. A nano flow cytometer for single lipid vesicle analysis. *Lab on a Chip* **17**, 830-841 (2017).

49.	Tegenfeldt, J.O. et al. The dynamics of genomic-length DNA molecules in 100-nm channels. *Proceedings of the National Academy of Sciences of the United States of America* **101**, 10979 (2004).

50.	Müller, V. & Westerlund, F. Optical DNA mapping in nanofluidic devices: principles and applications. *Lab on a Chip* **17**, 579-590 (2017).

51. Dill, F.H. Optical lithography. *IEEE Transactions on Electron Devices* **22**, 440-444 (1975).

52. Chou, S.Y., Krauss, P.R. & Renstrom, P.J. Nanoimprint lithography. *Journal of Vacuum Science & Technology B: Microelectronics and Nanometer Structures Processing, Measurement, and Phenomena* **14**, 4129-4133 (1996).

53. Quate, C.F. Scanning probes as a lithography tool for nanostructures. *Surface Science* **386**, 259-264 (1997).

54. Grigorescu, A.E. & Hagen, C.W. Resists for sub-20-nm electron beam lithography with a focus on HSQ: state of the art. *Nanotechnology* **20**, 292001 (2009).

55. Manfrinato, V.R. et al. Resolution Limits of Electron-Beam Lithography toward the Atomic Scale. *Nano Letters* **13**, 1555-1558 (2013).

56. Fu, Y.Q. et al. Deep reactive ion etching as a tool for nanostructure fabrication. *Journal of Vacuum Science & Technology B: Microelectronics and Nanometer Structures Processing, Measurement, and Phenomena* **27**, 1520-1526 (2009).

57. Levin, S. et al. A nanofluidic device for parallel single nanoparticle catalysis in solution. *Nature Communications* **10** (2019).

58. Park, S., Jung, S., Heo, J. & Hong, J. Facile synthesis of polysilsesquioxane toward durable superhydrophilic/superhydrophobic coatings for medical devices. *Journal of Industrial and Engineering Chemistry* **77**, 97-104 (2019).

59. Kim, K.-H., Jung, B. & Jeong, Y.-C. Foldable hard coating materials based on reaction-controlled polysilsesquioxane resin for flexible electronic devices. *Progress in Organic Coatings* **143**, 105639 (2020).

60. Gu, J., Gupta, R., Chou, C.-F., Wei, Q. & Zenhausern, F. A simple polysilsesquioxane sealing of nanofluidic channels below 10 nm at room temperature. *Lab on a Chip* **7**, 1198-1201 (2007).

61. Sriram, K.K., Nayak, S., Pengel, S., Chou, C.-F. & Erbe, A. 10 nm deep, sub-nanoliter fluidic nanochannels on germanium for attenuated total reflection infrared (ATR-IR) spectroscopy. *Analyst* **142**, 273-278 (2017).

62. Sriram, K.K., Yeh, J.-W., Lin, Y.-L., Chang, Y.-R. & Chou, C.-F. Direct optical mapping of transcription factor binding sites on field-stretched λ-DNA in nanofluidic devices. *Nucleic Acids Research* **42**, e85-e85 (2014).

63. Sriram, K.K., Chang, C.-L., Rajesh Kumar, U. & Chou, C.-F. DNA combing on low-pressure oxygen plasma modified polysilsesquioxane substrates for single-molecule studies. *Biomicrofluidics* **8**, 052102-052102 (2014).

64. Diaz Fernandez, Y.A. et al. The conquest of middle-earth: combining top-down and bottom-up nanofabrication for constructing nanoparticle based devices. *Nanoscale* **6**, 14605-14616 (2014).

65. Fu, X. et al. Top-down fabrication of shape-controlled, monodisperse nanoparticles for biomedical applications. *Advanced Drug Delivery Reviews* **132**, 169-187 (2018).

66. Xu, Y., Matsumoto, N., Wu, Q., Shimatani, Y. & Kawata, H. Site-specific nanopatterning of functional metallic and molecular arbitrary features in nanofluidic channels. *Lab on a Chip* **15**, 1989-1993 (2015).

67. Reichelt, K. Nucleation and growth of thin films. *Vacuum* **38**, 1083-1099 (1988).

68. Wu, H.-L. et al. A Comparative Study of Gold Nanocubes, Octahedra, and Rhombic Dodecahedra as Highly Sensitive SERS Substrates. *Inorganic Chemistry* **50**, 8106-8111 (2011).

69. Huang, W.-C., Lyu, L.-M., Yang, Y.-C. & Huang, M.H. Synthesis of Cu2O Nanocrystals from Cubic to Rhombic Dodecahedral Structures and Their Comparative Photocatalytic Activity. *Journal of the American Chemical Society* **134**, 1261-1267 (2012).

70. Das, M., Shim, K.H., An, S.S.A. & Yi, D.K. Review on gold nanoparticles and their applications. *Toxicology and Environmental Health Sciences* **3**, 193-205 (2011).

71. Reichenberger, S., Marzun, G., Muhler, M. & Barcikowski, S. Perspective of Surfactant-Free Colloidal Nanoparticles in Heterogeneous Catalysis. *ChemCatChem* **11**, 4489-4518 (2019).

72. Zheng, N., Fan, J. & Stucky, G.D. One-Step One-Phase Synthesis of Monodisperse Noble-Metallic Nanoparticles and Their Colloidal Crystals. *Journal of the American Chemical Society* **128**, 6550-6551 (2006).

73. Huang, X., Wu, H., Liao, X. & Shi, B. One-step, size-controlled synthesis of gold nanoparticles at room temperature using plant tannin. *Green Chemistry* **12**, 395-399 (2010).

74. Guo, J., Armstrong, M.J., O'Driscoll, C.M., Holmes, J.D. & Rahme, K. Positively charged, surfactant-free gold nanoparticles for nucleic acid delivery. *RSC Advances* **5**, 17862-17871 (2015).

75. Luo, S. et al. Sorption of Differently Charged Gold Nanoparticles on Synthetic Pyrite. *Minerals* **8** (2018).

76. Stolaś, A., Darmadi, I., Nugroho, F.A.A., Moth-Poulsen, K. & Langhammer, C. Impact of Surfactants and Stabilizers on Palladium Nanoparticle–Hydrogen Interaction Kinetics: Implications for Hydrogen Sensors. *ACS Applied Nano Materials* **3**, 2647-2653 (2020).

77. Bligaard, T. & Nørskov, J.K. Ligand effects in heterogeneous catalysis and electrochemistry. *Electrochimica Acta* **52**, 5512-5516 (2007).

78.   Burrows, N.D. et al. Surface Chemistry of Gold Nanorods. *Langmuir* **32**, 9905-9921 (2016).

79.   Zhou, S. et al. Enabling Complete Ligand Exchange on the Surface of Gold Nanocrystals through the Deposition and Then Etching of Silver. *Journal of the American Chemical Society* **140**, 11898-11901 (2018).

80.   Liu, J. et al. Fluorescent nanoparticles for chemical and biological sensing. *Science China Chemistry* **54**, 1157 (2011).

81.   Maier, O., Oberle, V. & Hoekstra, D. Fluorescent lipid probes: some properties and applications (a review). *Chemistry and Physics of Lipids* **116**, 3-18 (2002).

82.   Haupt, S., Lazar, I., Weitman, H., Senge, M.O. & Ehrenberg, B. Pdots, a new type of nanoparticle, bind to mTHPC via their lipid modified surface and exhibit very high FRET efficiency between the core and the sensitizer. *Physical Chemistry Chemical Physics* **17**, 11412-11422 (2015).

83.   Rideau, E., Dimova, R., Schwille, P., Wurm, F.R. & Landfester, K. Liposomes and polymersomes: a comparative review towards cell mimicking. *Chemical Society Reviews* **47**, 8572-8610 (2018).

84.   Mourdikoudis, S., Pallares, R.M. & Thanh, N.T.K. Characterization techniques for nanoparticles: comparison and complementarity upon studying nanoparticle properties. *Nanoscale* **10**, 12871-12934 (2018).

85.   Erni, R., Rossell, M.D., Kisielowski, C. & Dahmen, U. Atomic-Resolution Imaging with a Sub-50-pm Electron Probe. *Phys Rev Lett* **102**, 096101 (2009).

86.   Valeur, B. & Berberan-Santos, M.N. A Brief History of Fluorescence and Phosphorescence before the Emergence of Quantum Theory. *Journal of Chemical Education* **88**, 731-738 (2011).

87.   Atkins, P.W. & Jones, L. Chemical principles : the quest for insight, Edn. 3. ed. (Freeman, 2004).

88.   Atkins, P.W., De Paula, J. & Friedman, R.S. Quanta, matter, and change : a molecular approach to physical chemistry. (Oxford University Press, 2009).

89.   Skoog, D.A., Holler, F.J. & Nieman, T.A. Principles of instrumental analysis, Edn. 5., [rev. and updated] ed. (Saunders College Publishing, 1998).

90.   Lakowicz, J.R. Principles of fluorescence spectroscopy, Edn. Third edition. (Springer, 2006).

91.   Demchenko, A.P. Advanced Fluorescence Reporters in Chemistry and Biology II. [electronic resource] : Molecular Constructions, Polymers and Nanoparticles, Edn. 1st ed. 2010. (Springer Berlin Heidelberg, 2010).

92. Umezawa, K., Nakamura, Y., Makino, H., Citterio, D. & Suzuki, K. Bright, Color-Tunable Fluorescent Dyes in the Visible–Near-Infrared Region. *Journal of the American Chemical Society* **130**, 1550-1551 (2008).

93. Cordes, T. & Blum, S.A. Opportunities and challenges in single-molecule and single-particle fluorescence microscopy for mechanistic studies of chemical reactions. *Nature Chemistry* **5**, 993-999 (2013).

94. Glazer, A.N. & Rye, H.S. Stable dye–DNA intercalation complexes as reagents for high-sensitivity fluorescence detection. *Nature* **359**, 859-861 (1992).

95. Johnson, I. Review: Fluorescent probes for living cells. *The Histochemical Journal* **30**, 123-140 (1998).

96. Gessner, T. & Mayer, U. Triarylmethane and Diarylmethane Dyes. *Ullmann's Encyclopedia of Industrial Chemistry* (2000).

97. Levitus, M. Handbook of Fluorescence Spectroscopy and Imaging. From Ensemble to Single Molecules. Edited by Markus Sauer, Johan Hofkens and Jörg Enderlein. *Angewandte Chemie. International Edition* **50**, 9017-9018 (2011).

98. Kriss, T.C. & Kriss, V.M. History of the Operating Microscope: From Magnifying Glass to Microneurosurgery. *Neurosurgery* **42**, 899-907 (1998).

99. Jay, M.E. in Proc.SPIE, Vol. 3749 (1999).

100. Rayleigh XXXI. Investigations in optics, with special reference to the spectroscope. *The London, Edinburgh, and Dublin Philosophical Magazine and Journal of Science* **8**, 261-274 (1879).

101. Huang, B., Bates, M. & Zhuang, X. Super-Resolution Fluorescence Microscopy. *Annual Review of Biochemistry* **78**, 993-1016 (2009).

102. Ghauharali & Brakenhoff Fluorescence photobleaching-based image standardization for fluorescence microscopy. *Journal of Microscopy* **198**, 88-100 (2000).

103. Kreibig, U. & Vollmer, M. Optical Properties of Metal Clusters. [electronic resource], Edn. 1st ed. 1995. (Springer Berlin Heidelberg, 1995).

104. Jain, P.K., Lee, K.S., El-Sayed, I.H. & El-Sayed, M.A. Calculated Absorption and Scattering Properties of Gold Nanoparticles of Different Size, Shape, and Composition: Applications in Biological Imaging and Biomedicine. *The Journal of Physical Chemistry B* **110**, 7238-7248 (2006).

105. Berzelius, J.J. Årsberättelsen om framsteg i fysik och kemi. (1835).

106. Ostwald, W. Catalysis. *Phys. Zeitschrift* **3**, 313-322 (1901).

107. Chorkendorff, I. & Niemantsverdriet, J.W. Concepts of modern catalysis and kinetics, Edn. 2nd, rev. and enlarged ed. (Wiley-VCH, 2007).

108. van Leeuwen, P.W.N.M. & Chadwick, J.C. Homogeneous Catalysts: Activity – Stability – Deactivation. (Wiley-VCH Verlag GmbH & Co. KGaA, 2011).

109. Hagen, J. Industrial Catalysis : A Practical Approach. (John Wiley & Sons, Incorporated, Berlin, GERMANY; 2015).

110. Astruc, D. Introduction: Nanoparticles in Catalysis. *Chemical Reviews* **120**, 461-463 (2020).

111. Papp, C. From Flat Surfaces to Nanoparticles: In Situ Studies of the Reactivity of Model Catalysts. *Catalysis Letters* **147**, 2-19 (2017).

112. Biener, J., Biener, M.M., Madix, R.J. & Friend, C.M. Nanoporous Gold: Understanding the Origin of the Reactivity of a 21st Century Catalyst Made by Pre-Columbian Technology. *ACS Catalysis* **5**, 6263-6270 (2015).

113. Schlögl, R. Heterogeneous Catalysis. *Angewandte Chemie International Edition* **54**, 3465-3520 (2015).

114. Jones, R.O. Density functional theory: Its origins, rise to prominence, and future. *Reviews of Modern Physics* **87**, 897-923 (2015).

115. Akça, A., Genç, A.E. & Kutlu, B. BH4 dissociation on various metal (1 1 1) surfaces: A DFT study. *Applied Surface Science* **473**, 681-692 (2019).

116. Jinnouchi, R. & Asahi, R. Predicting Catalytic Activity of Nanoparticles by a DFT-Aided Machine-Learning Algorithm. *The Journal of Physical Chemistry Letters* **8**, 4279-4283 (2017).

117. Jørgensen, M. & Grönbeck, H. Scaling Relations and Kinetic Monte Carlo Simulations To Bridge the Materials Gap in Heterogeneous Catalysis. *ACS Catalysis* **7**, 5054-5061 (2017).

118. Rampino, L.D. & Nord, F.F. Preparation of Palladium and Platinum Synthetic High Polymer Catalysts and the Relationship between Particle Size and Rate of Hydrogenation. *Journal of the American Chemical Society* **63**, 2745-2749 (1941).

119. Haruta, M., Kobayashi, T., Sano, H. & Yamada, N. Novel Gold Catalysts for the Oxidation of Carbon Monoxide at a Temperature far Below 0 °C. *Chemistry Letters* **16**, 405-408 (1987).

120. Du, L. et al. Plasmon-Induced Charge Separation and Recombination Dynamics in Gold−TiO2 Nanoparticle Systems: Dependence on TiO2 Particle Size. *The Journal of Physical Chemistry C* **113**, 6454-6462 (2009).

121. Somorjai, G.A. The surface science of heterogeneous catalysis. *Surface Science* **299-300**, 849-866 (1994).

122. Chen, T. et al. Single-Molecule Nanocatalysis Reveals Facet-Dependent Catalytic Kinetics and Dynamics of Pallidium Nanoparticles. *ACS Catalysis* **7**, 2967-2972 (2017).

123. Zhou, X., Choudhary, E., Andoy, N.M., Zou, N. & Chen, P. Scalable Parallel Screening of Catalyst Activity at the Single-Particle Level and Subdiffraction Resolution. **3**, 1448-1453 (2013).

124. Zhou, X. et al. Quantitative super-resolution imaging uncovers reactivity patterns on single nanocatalysts. *Nature Nanotechnology* **7**, 237-241 (2012).

125. Xu, W., Kong, J.S., Yeh, Y.-T.E. & Chen, P. Single-molecule nanocatalysis reveals heterogeneous reaction pathways and catalytic dynamics. *Nature Materials* **7**, 992-996 (2008).

126. Tel-Vered, R. & Bard, A.J. Generation and Detection of Single Metal Nanoparticles Using Scanning Electrochemical Microscopy Techniques. *The Journal of Physical Chemistry B* **110**, 25279-25287 (2006).

127. Liu, R. et al. Atomic-Level-Designed Catalytically Active Palladium Atoms on Ultrathin Gold Nanowires. *Advanced Materials* **29**, 1604571 (2017).

128. Nie, S. & Emory, S.R. Probing Single Molecules and Single Nanoparticles by Surface-Enhanced Raman Scattering. *Science* **275**, 1102 (1997).

129. van Schrojenstein Lantman, E.M., Deckert-Gaudig, T., Mank, A.J.G., Deckert, V. & Weckhuysen, B.M. Catalytic processes monitored at the nanoscale with tip-enhanced Raman spectroscopy. *Nature Nanotechnology* **7**, 583-586 (2012).

130. Hartman, T., Wondergem, C.S., Kumar, N., van den Berg, A. & Weckhuysen, B.M. Surface- and Tip-Enhanced Raman Spectroscopy in Catalysis. *The Journal of Physical Chemistry Letters* **7**, 1570-1584 (2016).

131. Wu, C.-Y. et al. High-spatial-resolution mapping of catalytic reactions on single particles. *Nature* **541**, 511-515 (2017).

132. Neubrech, F., Huck, C., Weber, K., Pucci, A. & Giessen, H. Surface-Enhanced Infrared Spectroscopy Using Resonant Nanoantennas. *Chemical Reviews* **117**, 5110-5145 (2017).

133. Albinsson, D. et al. Operando detection of single nanoparticle activity dynamics inside a model pore catalyst material. *Science Advances* **6**, eaba7678 (2020).

134. Fritzsche, J. et al. Single Particle Nanoplasmonic Sensing in Individual Nanofluidic Channels. *Nano Letters* **16**, 7857-7864 (2016).

135. Wang, H., Zhang, T. & Zhou, X. Dark-field spectroscopy: development, applications and perspectives in single nanoparticle catalysis. *Journal of Physics: Condensed Matter* **31**, 473001 (2019).

136. Xu, W., Zhang, Y. & Chen, T. X-ray-Based Microscopy of Single Particle Nanocatalysis. 181-206 (2019).

137. Vendelbo, S.B. et al. Visualization of oscillatory behaviour of Pt nanoparticles catalysing CO oxidation. *Nature Materials* **13**, 884-890 (2014).

138. Jiang, Z.-J., Liu, C.-Y. & Sun, L.-W. Catalytic Properties of Silver Nanoparticles Supported on Silica Spheres. *The Journal of Physical Chemistry B* **109**, 1730-1735 (2005).

139. Wang, X., Pauli, J., Niessner, R., Resch-Genger, U. & Knopp, D. Gold nanoparticle-catalyzed uranine reduction for signal amplification in fluorescent assays for melamine and aflatoxin B1. *Analyst* **140**, 7305-7312 (2015).

140. Compton, R.G., Mason, D. & Unwin, P.R. Rotating-disc electrode voltammetry. Waveshape analysis for DISP2 and EC2 processes. *Journal of the Chemical Society, Faraday Transactions 1: Physical Chemistry in Condensed Phases* **84**, 473 (1988).

141. Compton, R.G., Mason, D. & Unwin, P.R. The reduction of fluorescein in aqueous solution (at pH 6). A new DISP2 reaction. *Journal of the Chemical Society, Faraday Transactions 1: Physical Chemistry in Condensed Phases* **84**, 483 (1988).

142. Coles, B.A. & Compton, R.G. Photoelectrochemical ESR. Part I. Experimental. *Journal of Electroanalytical Chemistry* **144**, 87-98 (1983).

143. Compton, R.G., Coles, B.A. & Pilkington, M.B.G. Photoelectrochemical electron spin resonance. Part 3.—The reduction of fluorescein: a 'photo-DISP2' reaction. *Journal of the Chemical Society, Faraday Transactions 1: Physical Chemistry in Condensed Phases* **84**, 4347 (1988).

144. Compton, R.G., Daly, P.J., Unwin, P.R. & Waller, A.M. In-situ electrochemical ESR: ECE versus dispi. *Journal of Electroanalytical Chemistry and Interfacial Electrochemistry* **191**, 15-29 (1985).

145. Compton, R.G. & Unwin, P.R. Channel and tubular electrodes. *Journal of Electroanalytical Chemistry and Interfacial Electrochemistry* **205**, 1-20 (1986).

146. Zhang, Y. et al. Superresolution fluorescence mapping of single-nanoparticle catalysts reveals spatiotemporal variations in surface reactivity. *Proceedings of the National Academy of Sciences of the United States of America* **112**, 8959-8964 (2015).

147. Mayer, K.M., Shnipes, J., Davis, D. & Walt, D.R. Catalytic kinetics of single gold nanoparticles observed via optical microwell arrays. *Nanotechnology* **26**, 055704 (2015).

148. Zhao, B., Summers, F.A. & Mason, R.P. Photooxidation of Amplex Red to resorufin: implications of exposing the Amplex Red assay to light. *Free Radic Biol Med* **53**, 1080-1087 (2012).

149. Li, W. et al. Single-Molecular Catalysis Identifying Activation Energy of the Intermediate Product and Rate-Limiting Step in Plasmonic Photocatalysis. *Nano Letters* **20**, 2507-2513 (2020).

150. Janick, J. Ancient Egyptian Agriculture and the Origins of Horticulture. *Acta Hort* **582** (2002).

151. Tabor, D. Gases, liquids and solids and other states of matter, Edn. 3. ed. (Cambridge Univ. Press, 1991).

152. Brown, R. XXVII. A brief account of microscopical observations made in the months of June, July and August 1827, on the particles contained in the pollen of plants; and on the general existence of active molecules in organic and inorganic bodies. *The Philosophical Magazine* **4**, 161-173 (1828).

153. Einstein, A. Über die von der molekularkinetischen Theorie der Wärme geforderte Bewegung von in ruhenden Flüssigkeiten suspendierten Teilchen. *Annalen der Physik* **322**, 549-560 (1905).

154. Gross-Rother, J., Blech, M., Preis, E., Bakowsky, U. & Garidel, P. Particle Detection and Characterization for Biopharmaceutical Applications: Current Principles of Established and Alternative Techniques. *Pharmaceutics* **12**, 1112 (2020).

155. Goldburg, W.I. Dynamic light scattering. *American Journal of Physics* **67**, 1152-1160 (1999).

156. Weatherall, E. & Willmott, G.R. Applications of tunable resistive pulse sensing. *Analyst* **140**, 3318-3334 (2015).

157. Minelli, C. et al. Measuring the size and density of nanoparticles by centrifugal sedimentation and flotation. *Analytical Methods* **10**, 1725-1732 (2018).

158. Macey, M.G. Flow Cytometry. [electronic resource] : Principles and Applications, Edn. 1st ed. 2007. (Humana Press, 2007).

159. Yang, D.T., Lu, X., Fan, Y. & Murphy, R.M. Evaluation of Nanoparticle Tracking for Characterization of Fibrillar Protein Aggregates. *AIChE J* **60**, 1236-1244 (2014).

160. Block, S., Fast, B.J., Lundgren, A., Zhdanov, V.P. & Höök, F. Two-dimensional flow nanometry of biological nanoparticles for accurate determination of their size and emission intensity. *Nature Communications* **7**, 12956 (2016).

161. Persson, F. et al. Lipid-Based Passivation in Nanofluidics. *Nano Letters* **12**, 2260-2265 (2012).

162. Dechadilok, P. & Deen, W.M. Hindrance Factors for Diffusion and Convection in Pores. *Industrial & Engineering Chemistry Research* **45**, 6953-6959 (2006).

163. van der Sman, R.G.M. Drag force on spheres confined on the center line of rectangular microchannels. *Journal of Colloid and Interface Science* **351**, 43-49 (2010).

164. Berglund, A.J. Statistics of camera-based single-particle tracking. *Physical Review E* **82**, 011917 (2010).

165. Sankir, M., Serin, R.B., Semiz, L. & Sankir, N.D. Unusual behavior of dynamic hydrogen generation from sodium borohydride. *International Journal of Hydrogen Energy* **39**, 2608-2613 (2014).

166. Chang, X., Batchelor-McAuley, C. & Compton, R.G. Hydrogen peroxide reduction on single platinum nanoparticles. *Chemical Science* **11**, 4416-4421 (2020).

167. Bell, T.E. & Torrente-Murciano, L. H2 Production via Ammonia Decomposition Using Non-Noble Metal Catalysts: A Review. *Topics in Catalysis* **59**, 1438-1457 (2016).

168. Naidu, D.K. & Fisher, R.B. in BMVC91. (ed. P. Mowforth) 217-225 (Springer London, London; 1991).

169. Lu, L., Zou, S. & Fang, B. The Critical Impacts of Ligands on Heterogeneous Nanocatalysis: A Review. *ACS Catalysis*, 6020-6058 (2021).

170. Albinsson, D. et al. Copper catalysis at operando conditions—bridging the gap between single nanoparticle probing and catalyst-bed-averaging. *Nature Communications* **11**, 4832 (2020).

171. Mao, X., Liu, C., Hesari, M., Zou, N. & Chen, P. Super-resolution imaging of non-fluorescent reactions via competition. *Nature Chemistry* **11**, 687-694 (2019).

172. Rodrigues, T.S., da Silva, A.G.M. & Camargo, P.H.C. Nanocatalysis by noble metal nanoparticles: controlled synthesis for the optimization and understanding of activities. *Journal of Materials Chemistry A* **7**, 5857-5874 (2019).